AD NUMBER

AD046678

NEW LIMITATION CHANGE

TO

Approved for public release, distribution unlimited

FROM

Distribution authorized to U.S. Gov't. agencies and their contractors; Administrative/Operational Use; Jan 1954. Other requests shall be referred to Wright Air Development Center, Wright-Patterson AFB, OH 45433.

AUTHORITY

AFAL ltr, 17 Aug 1979

WADC TECHNICAL REPORT 53-497

INVESTIGATION OF THE THWAITES AIRFOIL PRINCIPLE AS APPLIED TO HELICOPTER ROTOR BLADES

L. ARNOLD
S. W. YUAN

LEE ARNOLD ASSOCIATES, INC.

JANUARY 1954

WRIGHT AIR DEVELOPMENT CENTER

NOTICE

When Government drawings, specifications, or other data are used for any purpose other than in connection with a definitely related Government procurement operation, the United States Government thereby incurs no responsibility nor any obligation whatsoever; and the fact that the Government may have formulated, furnished, or in any way supplied the said drawings, specifications, or other data, is not to be regarded by implication or otherwise as in any manner licensing the holder or any other person or corporation, or conveying any rights or permission to manufacture, use, or sell any patented invention that may in any way be related thereto.

WADC TECHNICAL REPORT 53-497

INVESTIGATION OF THE THWAITES AIRFOIL PRINCIPLE AS APPLIED TO HELICOPTER ROTOR BLADES

L. Arnold
S. W. Yuan

Lee Arnold Associates, Inc.

January 1954

Aeronautical Research Laboratory
Contract No. AF33(616)-2087
RDO No. 465-5

Wright Air Development Center
Air Research and Development Command
United States Air Force
Wright-Patterson Air Force Base, Ohio

TABLE OF CONTENTS

LIST OF ILLUSTRATIONS

PURPOSE

The firm of Lee Arnold Associates presented a proposal to the Air Force which would initiate an experimental investigation of the merits of a novel helicopter rotor system. It was recommended at that time that a theoretical investigation be conducted in order to justify the initiation of such an experimental program. The results of the theoretical study are contained herein.

CONCLUSIONS

It is concluded from the foregoing that the use of the Kármán-Yuan rotor incorporating an oval shaped airfoil section, boundary layer suction, and flap control on a helicopter, would make possible substantial improvements in performance characteristics, including rate of vertical climb, forward flight speed and useful load lifting capacity.

It is further concluded that an experimental investigation is warranted in order to substantiate the findings presented in this report and to obtain information that could be applied to an actual design incorporating the Kármán-Yuan rotor features.

SUMMARY

A performance calculation has been carried out for the purpose of comparing the Piasecki XH-16 rotor with the Kármán-Yuan rotor. The two rotors were assumed identical in size and lifting capacity (rotor diameter = 82 ft, gross weight = 36600 lbs). The Piasecki rotor blade is equipped with an NACA 0015 airfoil and the Kármán-Yuan rotor blade with an elliptical airfoil of 18% thickness chord ratio and cyclic flap control. The controllable lift distribution along the blade span of the Kármán-Yuan rotor is achieved by varying the spanwise flap location and applied boundary layer suction. Due to the high lift coefficient employed in the Kármán-Yuan rotor blade it was found that a lower rotational speed can be used to sustain the same gross weight as does the XH-16.

The results of the calculations are summarized in the following tables.

Table 1 Piasecki XH-16 Helicopter (tip speed 630 ft/sec)

Rotor Horsepower	Induced	Profile	Parasite	Total
Hovering	1984	740	0	2726
160 MPH	410	843	1415	2668

Table 2 Kármán-Yuan Helicopter (tip speed 430 ft/sec)

Rotor Horsepower	Induced	Profile	Parasite	Suction	Total
Hovering	2020	137	0	250-350	2407-2507
160 MPH	410	179	1234	250-350	2073-2173

The rotor suction horsepower includes an equivalent power loss due to weight of suction equipment. The range of values of that term results from assuming maximum and minimum estimates corresponding to laminar and possible turbulent flow on the rotor blade.

It is seen from the above that the saving in rotor horsepower for the hovering case of the Kármán-Yuan rotor (over that of the Piasecki XH-16 rotor) is about 10% and the power saving at 160 MPH is about 20%. These favorable characteristics result from the lower rotational speed employed and from the lower profile drag coefficient on the blades achieved by suction of the boundary layer. This 10% saving in hovering flight corresponds to a 30% increase in payload for the helicopter under consideration. Alternatively, for the same gross weight the rate of climb of the Kármán-Yuan helicopter would exceed the Piasecki XH-16 by 80%.

In addition to bringing about a large power saving within the forward flight range of the Piasecki XH-16 helicopter, the Kármán-Yuan rotor would eliminate the present speed limitation of the conventional helicopter which would result from

(1) stalling of the retreating blades, and

(2) compressibility effects in the advancing blades.

The effect described in the above item (2) is due to the low tip speed and low peak of the potential velocity on the upper blade surfaces.

An aeroelastic investigation indicated that certain unusual aeroelastic characteristics were found to be inherent in the Thwaites airfoil, which it is believed could be circumvented by suitable structural design.

It should be noted that extremely conservative estimates were made in the computation of power requirements of the Kármán-Yuan rotor. It is felt that somewhat less conservative estimates would reveal sharply improved operating characteristics.

INTRODUCTION

This report presents the results of an investigation including a performance study and an aeroelastic investigation of a Piasecki XH-16 helicopter equipped with a Kármán-Yuan rotor. The performance study included the effect of replacing the conventional rotor system of the XH-16 helicopter by a Kármán-Yuan rotor.

The XH-16 is a twin rotored helicopter having 82 foot diameter rotors arranged in overlapping tandem and its physical dimensions and aerodynamic design characteristics are as follows:

Number of blades	3 per rotor
Blade chord (constant)	2.33 feet
Blade radius	41 feet
Rotor solidity	.0546
Blade airfoil section	NACA 0015
Gross weight	36654 pounds
Tip speed	636 feet/second
Power available	3020 horsepower

The Kármán-Yuan rotor is provided with a doubly symmetric blade section with a cyclic flap control (Patent Serial No. 346,326, 1953). The periodic variation of lift on the blade in forward flight is fulfilled by cyclic variation of flap position. The production of high lift is then independent of blade angle of attack and the separation of the flow is prevented by continuous suction of the boundary layer. The physical dimensions of the helicopter with Kármán-Yuan modifications are kept the same as the XH-16 but the difference in aerodynamic design characteristics resulting from use of higher lift coefficients are as follows:

Blade airfoil section	18% elliptical section
Tip speed	430 feet/second

In the vertical flight condition the average lift coefficient for the XH-16 rotor blade is .442 and for the Kármán-Yuan rotor blade it is assumed to be 1.0. This is feasible because of its non-stall characteristics. Due to the higher lift coefficient employed in the Kármán-Yuan rotor blade a 32.5% decrease in rotational speed can be used to sustain the same gross weight as the XH-16. In the comparison of vertical flight performance it is sufficiently accurate to assume that the rotor blades in both cases are ideally twisted.

It is shown in Section 5 that the induced powers consumed in any two rotors (identical in size) are approximately inversely proportional to their respective tip loss factors. Since the difference in tip loss of the above considered rotors is less than 2% their difference in induced power is very slight.

A greater saving in profile power consumption by the Kármán-Yuan rotor over that of the XH-16 results from the lower rotational speed employed by the former rotor and from its lower profile drag coefficient on the blades achieved by suction of the boundary layer. The justification of the profile drag coefficient used in the calculation of profile power for the Kármán-Yuan rotor was explained in Section 5. Because of this greater saving in profile power of the Kármán-Yuan rotor over that of the XH-16 a great increase in vertical rate of climb is achieved by the former helicopter system.

In the forward flight performance calculation especially at the cruising speed range the induced power consumption is only about 25% of the total power consumption. Because of a greater saving in profile power as well as parasite power due to the rotor blades by the Kármán-Yuan rotor over that of the XH-16, the total power consumption in forward flight is much less than that of the XH-16. The method used in forward flight performance calculation does not take into account the loss in the region of reverse flow. Since the reverse flow has no detrimental affect on the Kármán-Yuan rotor, it is evident that the performance comparison in the forward flight condition is conservative.

The suction power was calculated so as to be sufficient to compensate for all losses occurring in the flow system. In order to take into consideration the possibility of the flow becoming turbulent the actual suction quantity used in the present calculation was arbitrarily assumed to be $2\frac{1}{2}$ times higher than the calculated values. Extremely conservative assumptions were made throughout in estimating suction requirements.

LIST OF SYMBOLS

A	Cross section area of duct or mean semi-axis (Equation (8.10))
A_e	Effective projected area of both rotors
a	Semi-chord of airfoil, or slope of lift curve
$\bar{a}$	Center of rotation of airfoil aft of center line
$\bar{a}_\Delta$	Perturbation center of pressure
$\bar{a}_L$	Static center of pressure
$2b$	Thickness of airfoil, or twice the number of blades in rotor
b_1	Width of rectangular duct
c_o	$(a^2 - b^2)^{\frac{1}{2}}$
c	Blade chord
C_{d_o}	Section profile drag coefficient
C_α	Section torsional stiffness
C_f	Duct friction coefficient
C_L	Section lift coefficient
$\bar{C}_L$	Average lift coefficient over disc
$\bar{C}_{M(\beta,k)}$	Theodorsen moment fuction for ellipse
$\bar{C}_{P(\beta,k)}$	Equation (8.34)
C_Q	Section coefficient of flow through airfoil profile
C_{Q_i}	Induced torque coefficient
C_T	Thrust coefficient
d	Hydraulic diameter of duct

D_o	Profile drag
$\vec{F}$	Vector force (Equation (8.16))
Gap	Vertical distance between rotor disc planes
h_1	Depth of rectangular duct
h	Vertical deflection of blade section
$\hat{i},\hat{j},\hat{k}$	Unit cartesian vectors
k	Maximum assumed value of k_r
k_r	Suction coefficient (Equation (3.14))
K	Velocity profile parameter in boundary layer
l	Length of duct
$\bar{l}$	Oscillatory center of pressure (Page 47)
L	Steady aerodynamic lift (Equation (8.1))
$\vec{L}$	Vector moment (Equation (8.16))
M_α	Section torsional resisting moment
M_a	Steady aerodynamic moment about elastic axis of blade section
M_o	Steady aerodynamic moment about center of blade section
M_Γ	Aerodynamic moment due to wake vorticity
M_{nc}	Non-circulatory moment on airfoil rotating about elastic axis
M_{nco}	Non-circulatory moment about center of airfoil
P_{nc}	Non-circulatory force on airfoil rotating about elastic axis
P_{nco}	Non-circulatory force on airfoil rotating about center
P_p	Parasite power

P_{av}	Available rotor horsepower
P_o	Profile power
P_i	Induced power
P_Γ	Circulatory force (Equation (8.33))
p_x	Suction pressure due to lift
p_1	Duct pressure drop due to loss of momentum
p_2	Pressure drop in duct due to friction
p_3	Duct pressure due to centrifugal force
p_s	Pressure drop across porous skin
$\vec{q}$	Vector velocity (Equation (8.17))
Q	Equation (8.26)
Q_o	Profile torque or suction quantity
Q_i	Induced rotor torque
Q_T	Total suction quantity per rotor
Q_s	Suction quantity through porous skin per unit radial length of blade
R	Radius of rotor disc
R_e	Effective radius of rotor disc
R_ℓ	Reynolds Number
r	Radial location of a disc element
$s/2a$	Non-dimensional distance on airfoil from forward stagnation point
T	Rotor thrust or kinetic energy
U	Total flow through rotor disc or potential velocity

U_1	Velocity component of airfoil section in x direction (Figure 8.2)
U_c	Total flow through disc in vertical climb
U_o	Free stream velocity
U_d	Duct velocity
V'	Resultant flow through disc in forward flight
V_1	Velocity component of airfoil section in y direction (Figure 8.2)
V_{max}	Maximum velocity of forward flight
V_o	Suction velocity through airfoil skin
V_c	Vertical rate of climb
V_h	Horizontal component of total airflow through rotor
V_s	Suction velocity through equivalent rectangular duct walls
v	Average downwash velocity (Equation (6.2))
v_{hov}	Induced downwash in hovering
v_c	Induced downwash in vertical climb
v_{eq}	$(v_{hov})^2/U_c$ (equivalent downwash)
W	Total weight of helicopter
x	r/R or coordinate of a point in direction of major axis of airfoil
x_e, x_i	Effective working blade range (Equation (5.3))
Z	$(\theta^2 U_o)/2a\nu$
α	Angle of attack
β	Flap angle (subscript t for tip angle)
γ	Rotor tilt

δ	Measure of boundary layer thickness
δ^*	Displacement thickness
λ	$(V_o \delta)/\nu$
Λ	$(\delta^2/\nu)\, dU/ds$
ρ	Density of airstream
σ	Rotor solidity
φ	Inflow angle of blade element (subscript t for tip angle)
φ_{onc}	Non-circulatory potential on contour of airfoil
ψ_{onc}	Non-circulatory stream function on contour of airfoil
θ	Momentum thickness or polar angle of point on contour in ζ - plane (Page 41)
τ_o	Wall shearing stress
Ω	Angular velocity of rotor (Sections 5, 6, 7) or of blade section (Section 8)
$\vec{\Omega}$	Vector angular velocity (Equation (8.17))
ω	Frequency of oscillation of blade section (rad./sec.)
μ	Advance ratio of rotor in forward flight
ζ	Complex circle plane (Equations (8.11) and (8.12))

SECTION 1

SURVEY OF LITERATURE

1.1 GALCIT TESTS

A report, Reference (1), on a wind tunnel test of a 35% thick elliptical airfoil has been studied. The high lifting characteristics of the Thwaites type airfoil were substantiated, for a maximum lift coefficient of 7.3 was obtained.

However, this investigation was very limited; no measurements of drag were made, the suction was applied over the total surface of the airfoil, and was, consequently, greatly in excess of requirements. Consequently, no estimate of optimum suction power requirements was made available. Effects of flap chord variation and chord location were not investigated.

1.2 BRITISH INVESTIGATIONS

The British reports (References (2) and (3)) contain the underlying principles of the Thwaites type airfoil. This includes a method for determining profiles which could obtain uniform chordwise lift distributions.

However, there is practically no experimental information available except for some two-dimensional tests on circular cylinders, the purpose of which was to substantiate the basic principles. It was seen that the high lift coefficients predicted by theory could be realized and that wake drag was practically eliminated.

No suction measurements were made.

1.3 UNITED AIRCRAFT REPORTS

Various United Aircraft Reports were studied (References (4), (5), (6) and (7)). Only References (4) and (5) contained pertinent information.

Summaries of these reports follow:

1. U.A.C. Report No. R - 278, Reference (4). This report presents an investigation of the optimum arrangement for maximum lift and jet thrust of various slot and flap combinations. The results of tests of a two-dimensional NACA 23012 wing model equipped with pressure slots can be summarized as follows:

   1.a A maximum lift coefficient of 4.7 was reached with a $\frac{1}{2}\%$ chord plain slot at 75% chord, a $\frac{1}{2}\%$ chord lip type slot at 100% chord, flap angle of 60°, and wing pressure of $16x(\rho V^2/2)$.

   1.b An increase of quarter-chord moment coefficient, from $C_{m_{\frac{1}{4}}} = -0.285$ for the basic wing with flap and no slots ($C_{L\ max} = 2.14$) to $C_{m_{\frac{1}{4}}} = -1.10$ for wing with flaps and slots ($C_{L\ max} = 4.7$) is indicated.

   1.c The suction quantity coefficient $C_Q = .0094$ was obtained for $C_{L\ max} = 3.72$, and $C_Q = .031$ was obtained for $C_{L\ max} = 4.7$.

   1.d It is pointed out that the increased momentum due to the jet may reduce the drag.

2. U.A.C. Report No. R - 95374-3, Reference (5). This report presents an experimental investigation of the effect of trailing edge suction and pressure slots to the lift control of a wing. The purpose of this investigation is to apply this lift control scheme as a gust alleviation device. The results of the investigation can be summarized as follows:

   2.a For the purpose of alleviating the effect of most gusts for an average 300 mph flight a lift coefficient of 0.4 would be sufficient.

   2.b The most efficient configuration tested was the trailing edge pressure slot which produces a lift coefficient

increment of about 0.4 for a power coefficient of .005. Such a power coefficient would represent about 7 to 15% of the total airplane power. However, in order to produce a lift coefficient increment of about 1.4, a suction power coefficient of 0.8 is needed.

2.c The pitching moment increments were nearly independent of all variables except lift increments. The value for $d C_m/d C_L$ is about -0.3 which is very close to the value obtained in the same case of pressure slots and flaps.

It is believed that the mechanisms described in the above reports would not be suitable for application to helicopter rotors because of the large moment coefficients as compared to other high lift devices and high suction quantity coefficients accompanying the increase of lift coefficients.

1.4 CONCLUSIONS

The reports studied do not furnish the information that is required to evaluate the characteristics of the Thwaites type airfoil, as applied to helicopters, there are no other data available to accomplish this evaluation.

SECTION 2

VELOCITY DISTRIBUTION ABOUT AN ELLIPTICAL AIRFOIL

The velocity distribution for the potential flow around an elliptical airfoil can be calculated from the known complex potential for a circle with aid of the following transformation between a circle and an ellipse (see Reference (8)).

$$Z = \frac{1}{2}\left(z + \sqrt{z^2 - c_o^2} \right) \qquad 2.1$$

where $c_o^2 = a^2 - b^2$ and the expression $z = \cosh \zeta$ represents elliptical coordinates $\zeta = \xi + i\eta$, $x = a \cos \eta$ and $y = b \sin \eta$ (on the ellipse).

If the potential flow consists of a parallel and a circulatory flow, the velocity at any point on the elliptical airfoil, as determined by the above mentioned transformation can be written

$$\frac{U}{U_o} = \frac{(1 + b/a)\sin(\eta - \alpha) + C_L/2\pi}{\sqrt{\sin^2\eta + (b/a)^2 \cos^2\eta}} \qquad 2.2$$

$$C_L = 2\pi (1 + b/a) \sin(\alpha + \beta)$$

The first derivative of the velocity distribution is given by

$$\frac{\partial\left(\frac{U}{U_o}\right)}{\partial\left(\frac{S}{2a}\right)} = \left[\frac{2}{\sqrt{1 - (1 - b^2/a^2)\cos^2\eta}}\right]\left\{\frac{(1 + b/a)\cos(\eta - \alpha)}{\sqrt{\sin^2\eta + (b/a)^2\cos^2\eta}}\right.$$

$$\left. - \frac{\left[(1 + b/a)\sin(\eta - \alpha) + \frac{C_L}{2\pi}\right]\left[(1 - b^2/a^2)\sin 2\eta\right]}{2\left[\sin^2\eta + (b/a)^2\cos^2\eta\right]^{3/2}}\right\} \qquad 2.3$$

The value of s/2a corresponding to a given value of η is determined from the integral

$$\frac{s}{2a} - \frac{s_o}{2a} = \int_{\eta_o}^{\eta} \sqrt{\sin^2\eta + b^2/a^2 \cos^2\eta}\, d\eta$$

which is easily evaluated by means of elliptic integrals.

The coordinates of the stagnation points for any given C_L and α can be determined by the following expressions:

$$\frac{x}{a} = \cos\eta_o = \frac{C_L \sin\alpha}{2\pi(1+b/a)} + \cos\alpha\sqrt{1 - \frac{C_L^2}{4\pi^2(1+b/a)^2}} \qquad 2.4$$

$$\frac{y}{b} = \sin\eta_o = \frac{-C_L \cos\alpha}{2\pi(1+b/a)} + \sin\alpha\sqrt{1 - \frac{C_L^2}{4\pi^2(1+b/a)^2}}$$

The nomenclatures in Equations (2.1), (2.2), (2.3) and (2.4) are explained in Figures 2.1 and 2.2.

The velocity distributions for the potential flow around an elliptical airfoil of 17.36% thickness chord ratio and C_L = 1, 2, 4 and α = 0 are calculated and shown in Figures 2.3, 2.4 and 2.5, respectively. The corresponding first derivative of the velocity distributions are given in Figures 2.6, 2.7 and 2.8, respectively. It will be noted that the velocities and gradients are given only for the forward half of the ellipse (top and bottom) since they are respectively symmetric and antisymmetric with respect to the vertical center line.

SECTION 3

CALCULATION OF SUCTION QUANTITY

In the previous section a potential flow is calculated about an elliptical airfoil for any given lift coefficient and the location on the airfoil of the dividing streamlines is determined. If a flap is placed along the calculated rear dividing streamline (at the stagnation point), the steady flow of real fluid past the airfoil will approximate closely to the calculated potential flow with circulation (References (1) and (2)). In order to prevent separation which would destroy the high lift, continuous suction must be applied along the surface of the airfoil where a positive pressure gradient exists.

If a one-parameter family for the velocity profile in the boundary layer is chosen, the following differential equation for non-dimensional momentum thickness is obtained from the Kármán Momentum Equation

$$\frac{dZ}{d\left(\frac{s}{2a}\right)} = \frac{2g(K)}{\left(\frac{U}{U_0}\right)}\left[\lambda - 2\Lambda g(K) - \Lambda\left\{1+\left(\frac{6}{\pi}-2\right)K\right\} + \left\{1+\left(1-\frac{\pi}{6}\right)K\right\}\right] \qquad 3.1$$

where

$$Z = \frac{\theta^2 U_0}{2a\nu}$$

$$g(K) = \frac{\theta}{\delta} = \frac{1}{2} + 0.06656\,K - 0.02358\,K^2$$

$$\frac{\delta^*}{\delta} = 1 + \left(\frac{6}{\pi}-2\right)K$$

$$K = \frac{\Lambda - \lambda - 1}{1+\left(1-\frac{\pi}{6}\right)\lambda} \qquad 3.2$$

$$\Lambda = \frac{\delta^2}{\nu}\frac{dU}{ds}$$

$$\lambda = \frac{V_0\,\delta}{\nu}$$

The differential equation for momentum thickness without suction can be obtained from Equation (3.1) by putting $\lambda = 0$ and $K = \Lambda - 1$, which gives

$$\frac{dZ}{d\left(\frac{s}{2a}\right)} = \frac{2g(\Lambda)\, f(\Lambda)}{U/U_o} \qquad 3.3$$

where

$$g(\Lambda) = \theta/\delta = 0.4099 + 0.1137\Lambda - 0.02358\Lambda^2$$

$$f(\Lambda) = 0.5236 - 1.433\Lambda - 0.1373\Lambda^2 + .04716\Lambda^3 \qquad 3.4$$

From the expressions for Λ and Z, (Equation (3.1)) and (Equation (3.2)), we obtain

$$Z \frac{d\left(\frac{U}{U_o}\right)}{d\left(\frac{s}{2a}\right)} = \Lambda g^2(\Lambda) \qquad 3.5$$

Equations (3.3) and (3.5) are the parametric representation of a first order differential equation in Z(s). They may be solved by procedures such as the isocline method provided the velocity distribution U and dU/ds and the initial values of Λ_o and $\left(dZ/ds\right)_o$ at the forward stagnation point S_o, are known. It is shown in Reference (8) that

$$\Lambda_o = .3547$$

$$Z_o = \frac{.0719}{\frac{d\left(\frac{U}{U_o}\right)}{d\left(\frac{s}{2a}\right)}} \qquad 3.6$$

$$\left[\frac{dZ}{d\left(\frac{s}{2a}\right)}\right]_o = \frac{\left[\frac{d^2\left(\frac{U}{U_o}\right)}{d\left(\frac{s}{2a}\right)^2}\right]}{\left[\frac{d\left(\frac{U}{U_o}\right)}{d\left(\frac{s}{2a}\right)}\right]^2}$$

The numerical solution of the pair of Equations (3.3) and (3.5) can be considerably simplified by eliminating the parameter Λ. This may be done by plotting 2fg versus Λg^2 and fitting straight line segments to various portions of the curve. It was found that the single straight line

$$2fg = .47 - 6.53 \Lambda g^2 \qquad 3.7$$

is sufficiently accurate in the range of Λ encountered. Substituting Equations (3.3) and (3.5) into (3.7) we have the first order, linear differential equation

$$\frac{dZ}{d\left(\frac{s}{2a}\right)} + \frac{6.53}{\left(\frac{U}{U_0}\right)}\left[\frac{d\left(\frac{U}{U_0}\right)}{d\left(\frac{s}{2a}\right)}\right] Z = \frac{.47}{\left(\frac{U}{U_0}\right)} \qquad 3.8$$

This has the solution

$$Z = \left(\frac{U}{U_0}\right)^{-6.53}\left[.47\int_{\frac{s_0}{2a}}^{\frac{s}{2a}}\left(\frac{U}{U_0}\right)^{5.53} d\left(\frac{s}{2a}\right) + Z_0\left(\frac{U}{U_0}\right)_0^{6.53}\right] \qquad 3.9$$

The second term in the bracket is zero when S_0 is a stagnation point, but must be included in other non-suction regions.

The solution, Equation (3.9) is obtained by simple quadratures in the region of positive velocity gradient, $dU/ds > 0$. At the minimum pressure point, at which the potential velocity gradient becomes zero, $dU/ds = 0$, the velocity profile inside the boundary layer approaches the flat plate velocity profile ($K = -1$). If the parameter K in Equations (3.1) and (3.2) is kept constant and equal to -1, the velocity distribution in the boundary layer will remain constant along the body in the flow. Equation (3.1) can then be reduced to the form

$$\frac{dZ}{d\left(\frac{s}{2a}\right)} = \frac{.429}{\left(\frac{U}{U_0}\right)} \qquad 3.10$$

which has the simple integral

$$Z = .429 \int_{(s/2a)_i}^{\frac{s}{2a}} \frac{d\left(\frac{s}{2a}\right)}{\left(\frac{U}{U_0}\right)} + Z_i \qquad 3.11$$

where S_i is the distance along the body to the initial point at which the suction is begun and Z_i is the corresponding value of Z, determined from the solution of Equation (3.9).

The above calculations are, of course, valid only up to the transition region, as Equation (3.1) does not apply to turbulent flow. In regard to the transition Reynolds Number at which flow may become turbulent, it can only be said at this time, that due to the favorable velocity profile secured by use of suction, the critical Reynolds Number becomes much higher than for the case without suction. The above interpretation is based on the theory of the stability of the laminar boundary layer, as in Reference (10).

Equation (3.9) gives the non-dimensional momentum thickness as a function of velocity in the potential flow and the initial values at which the application of suction begins. Since all the items are given in non-dimensional form, the value of the non-dimensional momentum thickness calculated from Equation (3.9) is unrestricted as to free stream velocity, length of chord, and the viscosity of the air.

For a given thickness to chord ratio of an airfoil, the non-dimensional velocity distribution in the potential flow can be computed as a function of the non-dimensional arc length. The non-dimensional momentum thickness in the region where suction is not needed is calculated from Equation (3.9). The suction is then applied at the minimum pressure point, and Equation (3.11) is used to calculate the momentum thickness. The initial values Z_i, (U_i/U_0) and $(s/2a)_i$ in Equation (3.11) occur at the end point of the solution, Equation (3.9).

The suction velocity V_0 necessary to maintain a constant shape of the velocity profile in the boundary layer can be derived from Equation (3.2), which gives

$$\frac{V_0}{U_0}\sqrt{R_\ell} = \frac{\Theta\sqrt{U_0/2a\nu}}{\left[1+(1-\pi/6)K\right]g(K)} \frac{d\left(\frac{U}{U_0}\right)}{d\left(\frac{s}{2a}\right)} - \frac{K+1}{1+(1-\pi/6)K} \frac{g(K)}{\Theta\sqrt{U_0/2a\nu}} \qquad 3.12$$

where R_ℓ is the Reynolds Number with reference to the chord of the airfoil. The value for $\theta\sqrt{U_o/2a\nu}$ in Equation (3.12) is obtained from Equation (3.9).

The resulting curves of momentum thickness versus the arc length of the airfoil are shown in Figures 3.1, 3.2, 3.3; and the suction velocities are shown in Figures 3.4, 3.5, 3.6 for $C_L = 1, 2, 4$, respectively.

The suction quantity needed in order to maintain the flat-plate velocity profile in the boundary layer after the minimum pressure point, can be determined from Equation (3.12). The coefficient of suction quantity C_Q can then be found by the following expression

$$C_Q = \sum \left(\frac{V_o}{U_o}\right) \Delta\left(\frac{s}{2a}\right) \qquad 3.13$$

Equation (3.13) can be expressed in the form

$$C_Q = \frac{k_r}{\sqrt{R_\ell}} \qquad 3.14$$

A maximum value of $k_r = 3.33$ will be used in Section 7.2 to obtain the suction quantity Q_o. This value os obtained from Figures 3.4, 3.5, and 3.6.

SECTION 4

CALCULATION OF PROFILE DRAG

The surface profile drag on the given airfoil can be calculated from the solution of laminar boundary layer theory given in the previous section. From the following momentum equation for the boundary layer with pressure gradient and suction

$$U^2 \frac{d\theta}{ds} + \left(2 + \frac{\delta^*}{\theta}\right)\theta U \frac{dU}{ds} = UV_o + \frac{\tau_o}{\rho} \qquad 4.1$$

we have

$$\sqrt{R_\ell}\ \frac{\tau_o}{\frac{1}{2}\rho U_o^2} = 2\left(\frac{U}{U_o}\right)\left[\frac{U}{U_o}\frac{d\sqrt{z}}{d(s/2a)} + \left(2+\frac{\delta^*}{\theta}\right)\sqrt{z}\ \frac{d\left(\frac{U}{U_o}\right)}{d\left(\frac{s}{2a}\right)} - \frac{V_o}{U_o}\sqrt{R_\ell}\right] \qquad 4.2$$

For $v_o \neq 0$ and $K = -1$, Equation (4.2) is reduced to the following expression

$$\frac{\tau_o}{\frac{1}{2}\rho U_o^2}\sqrt{R_\ell} = \frac{\left(U/U_o\right)^2}{\sqrt{z}}\ \frac{dz}{d(s/2a)} = \frac{0.4292}{\sqrt{z}}\left(\frac{U}{U_o}\right) \qquad 4.3$$

For $v_o = 0$, the following equation for friction drag is obtained.

$$\frac{\tau_o}{\frac{1}{2}\rho U_o^2}\sqrt{R_\ell} = \frac{2\left(\frac{U}{U_o}\right)}{\sqrt{z}}\left[\frac{1}{2}\frac{U}{U_o}\frac{dz}{d\left(\frac{s}{2a}\right)} + \left(2+\frac{\delta^*}{\theta}\right)z\ \frac{d\left(\frac{U}{U_o}\right)}{d\left(\frac{s}{2a}\right)}\right] \qquad 4.4$$

The coefficient of friction drag is

$$C_{do} = \frac{1}{\rho a U_o^2}\left[\int_{\text{Upper Surface}} \tau_o\, dx + \int_{\text{Lower Surface}} \tau_o\, dx\right] \qquad 4.5$$

Substituting the results of Equations (4.3) and (4.4) into Equation (4.5) yields the following numerical results.

C_L	1	2	4
C_{d_o}	$\frac{3.44}{\sqrt{R_\ell}}$	$\frac{4.25}{\sqrt{R_\ell}}$	$\frac{6.00}{\sqrt{R_\ell}}$

The above results are plotted in Figure 4.1. A linear relationship is indicated between the profile drag and lift coefficients, and a value of $C_{d_o}\sqrt{R_\ell} = 2.55$ is thereby found for $C_L = 0$.

It must be borne in mind that the above estimates are based on laminar flow theory. It is likely that part of the flow in the neighborhood of the rear stagnation point might become turbulent and that the actual friction coefficient may become two to three times greater than the above calculated values.

In order to justify the above conclusions, the same method was used to calculate the profile drag coefficient for the NACA 0015 airfoil. For laminar flow with suction it gives $\sqrt{R_\ell}C_{d_o} = 3.02$ for $C_L = 0.5$. The elliptical airfoil considered in the present report gives $\sqrt{R_\ell}C_{d_o} = 3.0$ for the same lift coefficient.

The profile drag coefficient of the NACA 0015 airfoil was then calculated for the case of zero suction and consequent turbulent boundary layer in the region of positive pressure gradient with the result $C_{d_o} = .0107$ for $R_\ell = 4.7 \times 10^6$. For a Reynolds Number very close to that value, the experimental value of the profile drag coefficient for NACA 0015 is .00928, thereby showing close agreement.

In view of the above comparison it is reasonable to assume that the calculated values of the profile drag coefficients may be multiplied by a factor of 3.5 in the estimation of performance of the Kármán-Yuan rotor when the elliptical airfoil is used in order to take into account the possibility of turbulent flow.

SECTION 5

STUDY OF THE EFFECT OF THE KÁRMÁN-YUAN ROTOR MODIFICATION ON THE PIASECKI XH-16 HELICOPTER VERTICAL FLIGHT PERFORMANCE

In the present section a comparison of vertical flight performance between the Piasecki XH-16 helicopter and the proposed Kármán-Yuan modification was made. Since there is no test data available on the Kármán-Yuan rotor, it is not justified at the present to make a detailed comparison such as effects at various altitudes, and Mach Number corrections. It is sufficient to assume that the blades are ideally twisted for both above mentioned rotors, and that they are both operated at sea level conditions.

5.1 RELATION BETWEEN THRUST AND INDUCED POWER

The differential thrust expression for a rotor having b blades can be obtained from the blade-element theory as follows.

$$dT = \frac{b}{2} \rho \Omega^2 r^2 C_L c \, dr \qquad 5.1$$

For the case of ideal twist

$$C_L = a \sin(\beta - \varphi) \simeq \frac{aR}{r} (\beta_t - \varphi_t) \qquad 5.2$$

where β is the flap angle defined in Section 2 and φ is the inflow angle of a blade element. The subscript $(\,)_t$ represents the condition at the tip of the blade. c and a are respectively the chord and $dC_L/d\alpha$.

Substituting Equation (5.2) into Equation (5.1) and replacing r/R by x, the total expression for thrust becomes

$$T = \int_{x_i}^{x_e} \frac{bc}{2} \rho \Omega^2 R^3 a (\beta_t - \varphi_t) x \, dx = \frac{bc}{4} \rho (\Omega R)^2 R a (\beta_t - \varphi_t)(x_e^2 - x_i^2) \qquad 5.3$$

The limits of the integral are taken within the effective working blade range x_i to x_e. Equating Equation (5.3) to

$$T = C_T \pi R^2 \rho (\Omega R)^2$$

the expression for thrust coefficient becomes

$$C_T = \frac{\sigma}{4} a (\beta_t - \varphi_t) \qquad 5.4$$

If $\bar{C}_L$ represents the average lift coefficient on a blade the expression for thrust coefficient may be written as follows.

$$C_T = \frac{\sigma}{6} \bar{C}_L (X_e^3 - X_i^3) \qquad 5.5$$

The inflow angle at the tip of a blade can be obtained from the combined momentum and blade-element theories which gives

$$\varphi_t = \sqrt{\frac{C_T}{2(X_e^2 - X_i^2)}} \qquad 5.6$$

The flap angle at the tip of a blade is obtained from the Equations (5.4) and (5.6) as follows.

$$\beta_t = \frac{4 C_T}{\sigma a (X_e^2 - X_i^2)} + \sqrt{\frac{C_T}{2(X_e^2 - X_i^2)}} \qquad 5.7$$

The induced part of the rotor torque which is caused by the components of the lift vectors in the plane of rotation is written as

$$Q_i = C_{Q_i} \pi R^3 \rho (\Omega R)^2 = \int_0^{X_e} \frac{b}{2} \rho (\Omega r)^2 a \left(\frac{R}{r}\right)^2 (\beta_t - \varphi_t) \varphi_t c r dr \qquad 5.8$$

Upon substitution of $\beta_t - \varphi_t$ and φ_t from Equations (5.4) and (5.6) into Equation (5.5) the coefficient of induced torque becomes

$$C_{Q_i} = \frac{C_T^{3/2}}{\sqrt{2}} \frac{X_e^2}{(X_e^2 - X_i^2)^{3/2}} \qquad 5.9$$

The induced power per rotor is given by the following expression.

$$P_i = \frac{1}{550} C_{Qi} \rho \pi R^2 (\Omega R)^3 \qquad 5.10$$

5.1.1 Induced Power Calculation for Piasecki XH-16 Rotor

5.1.1 (a) Rotor characteristics

Gross weight	36654 (twin rotors)
Tip speed	636 ft/sec
Blade chord	2.33 ft
Rotor diameter	82 ft
Rotor solidity	.0546

5.1.1 (b) The thrust, torque and induced power coefficients are computed;

$$C_T = \frac{W/2}{\rho \pi R^2 (\Omega R)^2} = .00362$$

$$X_e = 1 - \frac{\sqrt{2C_T}}{b} = .971 \quad ; \quad X_i = .2$$

$$\bar{C}_l = \frac{6 C_T}{\sigma} \frac{1}{(X_e^3 - X_i^3)} = .442$$

$$C_{Qi} = \frac{C_T^{3/2}}{\sqrt{2}} \frac{X_e^2}{(X_e^2 - X_i^2)^{3/2}} = .0001696$$

$$P_i = \frac{1}{550} C_{Qi} \rho \pi R^2 (\Omega R)^3 = 992 \text{ HP/rotor}$$

The induced power of a single XH-16 rotor (7° blade twist) was calculated in Reference (12) to be 1004 HP. The variation of the blade angle and the inflow angle along the blade are shown in Figure 5.1.

5.1.2 Induced Power Calculation for Kármán-Yuan Rotor

In the present comparison the average lift coefficient of 1.0 is assumed for the elliptical-flap airfoil system. With this average lift coefficient, the thrust coefficient for the rotor is

$$C_T = \frac{\bar{C}_L \sigma}{6}\left(x_e^3 - x_i^3\right) = .00907\, x_e^3 - .0000726$$

Substituting $C_T = 4.5(1 - x_e^2)$ into the above equation a cubic equation for x_e yields the following solution.

$$x_e = .958$$

$$C_T = .00791$$

In order to keep the same rotor thrust and rotor diameter, the tip speed of the Kármán-Yuan rotor becomes

$$\Omega R = \sqrt{\frac{T}{C_T \rho \pi R^2}} = 430 \text{ ft/sec.}$$

as compared to $\Omega R = 636$ ft/sec for the XH-16.
The induced torque coefficient is

$$C_{Q_i} = \frac{C_T^{3/2}}{\sqrt{2}} \frac{x_e^2}{(x_e^2 - x_i^2)^{3/2}} = .0005575$$

and the induced power per rotor is

$$P_i = \frac{1}{550} C_{Q_i} \rho \pi R^2 (\Omega R)^3 = 1012 \text{ HP}$$

The variation of the flap angle and the inflow angle along the blade are shown in Figure 5.2.

It will be noted that the ratio of the induced power of two different rotors can be expressed by the following simple

expression

$$\frac{P_{i1}}{P_{i2}} = \frac{X_{e1}^2 (X_{e2}^2 - X_i^2)^{3/2}}{X_{e2}^2 (X_{e1}^2 - X_i^2)^{3/2}}$$

Approximately, the induced power ratio of two different rotors is inversely proportional to the ratio of their tip loss factors. Since the difference in the tip loss ratios is less than 2%, the difference in induced power is also less than 2%.

5.2 PROFILE POWER

The differential profile drag expression for a rotor having b blades is

$$dD_o = b \frac{\rho}{2} (\Omega r)^2 C_{do} c\, dr \qquad 5.11$$

where C_{d_o} is the profile drag coefficient of the blade section.

Thus the differential power required to overcome the profile drag of b blade elements is

$$dP_o = \frac{1}{550} C_{do} \frac{\rho}{2} \sigma \pi R^2 (\Omega R)^3 x^3 dx \qquad 5.12$$

5.2.1 Profile Power for XH-16 Rotor

In Reference (12) a value of $C_{d_o} = .00928$ was used to calculate the profile power of the XH-16 rotor giving

$$P_o = \frac{1}{550} \left[.00928 \rho/2 \sigma \pi R^2 (\Omega R)^3\right] \int_o^1 x^3 dx$$

$$= 371 \text{ HP/rotor}$$

5.2.2 Profile Power for the Kármán-Yuan Rotor

The profile drag coefficient of an elliptical airfoil-flap system was calculated in Section 4 and it can be expressed by the following equation

$$C_{do} = \frac{2.55 + 0.853\, C_L}{\sqrt{R_\ell}} \qquad (5.13)$$

where

$$R_\ell = \frac{(\Omega R)c}{\nu} x = \frac{(430)(2.33)}{1.6 \times 10^{-4}} x = 6.25 \cdot 10^{-6} x$$

$$C_L = \frac{a}{x}(\beta_t - \varphi_t) = \frac{7.2}{x}(.092)$$

Since the profile torque is given by

$$Q_o = C_{Qo} \pi R^3 (\Omega R)^2$$

or

$$Q_o = \frac{\sigma}{2} \pi \rho R^3 (\Omega R)^2 \int_o^1 C_{do} x^3 dx \qquad (5.14)$$

the profile torque coefficient becomes

$$C_{Qo} = \frac{\sigma}{2}(10^{-3}) \int_o^1 [x^{5/2} + 0.226 x^{3/2}] dx = .0015 \frac{\sigma}{8} \qquad (5.15)$$

Hence the rotor profile drag coefficient of the Kármán-Yuan rotor is .0015.

In order to be conservative the profile drag coefficient used in the calculation of the profile power was assumed to be .0055 thereby accounting for possible turbulence. We obtain

$$P_o = \frac{1}{550}\left[\frac{\sigma}{8}(.0055\,\pi\rho R^2(\Omega R)^3\right] = 68.5 \text{ HP/rotor}$$

5.3 SUCTION POWER FOR THE KÁRMÁN-YUAN ROTOR

The power required for boundary layer suction, sufficient to maintain a given flow condition and lift distribution along the rotor blades is discussed in detail in Section 7. The total suction power required per rotor is found to be 175 HP.

5.4 SUMMARY OF ROTOR HORSEPOWER FOR HOVERING

	P_i	P_o	$P_{suction}$	P_{total}
Reference Section	(5.1)	(5.2)	(7.2)	
Piasecki XH-16	992	371	0	1363
Kármán-Yuan	1012	68.5	175	1255.5

% of Power Saving by Kármán-Yuan Rotor $= \frac{1363-1255.5}{1363} = 9.2\%$

The above power saving is equivalent to a 30% increase in payload.

5.5 COMPARISON OF VERTICAL CLIMB PERFORMANCE

The vertical rate of climb is computed by comparing the total flow through the disc, U, with the downwash velocity v. The difference between these two values is the rate of climb.

It is shown in Reference (12) that the rate of vertical climb, V_c, is related to the induced downwash in hovering, v_{hov}, and to the total flow through the disc in vertical climb, U_c, by the approximate formula

$$V_c = U_c - \frac{v_{hov}^2}{U_c} \qquad 5.16$$

where

$$U_c = 550 \frac{P_{AV} - P_o}{W}$$

and

$$v_{hov} = 550 \frac{P_i}{W}$$

Therefore the vertical rate of climb in feet per minute becomes

$$V_c = 60 (U_c - v_{eq}) \qquad 5.17$$

where

$$v_{eq} = \frac{v_{hov}^2}{U_c}$$

The resulting characteristics of the two rotors are listed below.

XH-16 Helicopter (Twin Rotors)

P_i 1984 HP (from Section 6.1.1)

P_o 742 HP (from Section 6.2.1)

v_{hov} $550\ P_i/W = 29.8$ ft/sec

P_{av} 3020 HP (from Reference (12), available HP)

U_c $550\ \frac{(P_{av} - P_o)}{W} = 34.2$ ft/sec

v_{eq} $(v_{hov}^2)/U_c = 26$ ft/sec

V_c $60\ (U_c - v_{eq}) = 492$ ft/min

Kármán-Yuan Helicopter Modification (Twin Rotors)

P_i 2024 HP (from Section 6.1.2)

P_o 137 HP (from Section 6.2.2)

P_{av} $3020 - 350 = 2670$ HP

v_{hov} $550\ P_i/W = 30.4$ ft/sec

v_{eq} $(v_{hov}^2)/U_c = 24.3$ ft/sec

V_c $60\ (U_c - v_{eq}) = 821$ ft/min

% increase in V_c by Kármán-Yuan Helicopter Modification = 79.5%

5.6 POWER-OFF DESCENT

In case of power failure, it is necessary for a helicopter to glide in autorotation with a low descent speed. In general, the blade angle of attack as well as the blade lift coefficient required for autorotation must be comparatively small. This can be accomplished in the Kármán-Yuan rotor by decreasing the angle β to a small magnitude i.e., by moving the flaps close to the trailing edge of the blades. Since the lift coefficient is comparatively small, the suction required can be relatively small. It appears that this small suction can be accomplished as a result of the combined centrifugal and tip venturi effects discussed in Section 7. Since the rate of descent of a helicopter depends to a great extent on the rotor profile drag, it is clear that the lower profile drag of the Kármán-Yuan rotor resulting from suction would lower the rate of descent.

SECTION 6

STUDY OF THE EFFECT OF THE KARMAN-YUAN ROTOR MODIFICATION ON THE PIASECKI XH-16 HELICOPTER FORWARD FLIGHT PERFORMANCE

The method used in the calculation of forward flight performance is based on the outline given in References (12) and (14). Since this method does not take into account the loss of efficiency in the reverse flow region, and the Kármán-Yuan rotor does not suffer this loss, it is evident that results calculated in the present section are conservative.

6.1 INDUCED POWER

The induced power in the region of forward speeds of particular interest (from that of best climb to V_{max}) represents only a relatively small fraction (1/3 to 1/5) of the total power required, hence the method based on momentum theory is sufficiently accurate for practical prediction of the induced power.

The induced power which is required to compensate for the energy carried away by the slipstream when downwash is produced can be expressed in horsepower as

$$P_i = \frac{Wv}{550} \qquad 6.1$$

where W is the weight supported by the rotor and v is the induced velocity. By analogy with fixed wing aircraft the average downwash may be found as a function of the area of the cross section of a stream tube having as its diameter the rotor span 2R. Thus, for a single rotor helicopter the average downwash velocity is

$$v = \frac{W}{2\pi R^2 \rho V'} \qquad 6.2$$

where V' is the resultant flow through the disc and may be expressed as

$$V' = V_h + v + V_h \gamma$$

where γ is the tilt of the rotor disc. However, since for the region of low and moderate flying speeds $V_h\gamma$ is small in comparison with v, while for high flying speeds the influence of all axial components (v and $V_h\gamma$) are unimportant compared to V_h, for all practical purposes the resultant V' can be expressed approximately as

$$V' = \sqrt{V_h^2 + v^2} \qquad 6.3$$

When the rotors are arranged in close tandem, however, it is evident that the average induced velocity will increase due to their proximity. The thrust of a tandem rotored helicopter may be expressed

$$T = 2\rho v \sqrt{V_h^2+v^2}\left[(\pi R_e^2 + 2R_e \times Gap) + \left\{A_e - (\pi R_e^2 + 2R_e \times Gap)\right\}\frac{v}{\sqrt{V_h^2+v^2}}\right] \qquad 6.4$$

where A_e is the effective projected area of both rotors, R_e is the effective rotor radius, and V_h is the horizontal component of the total air flow and Gap is the vertical distance between rotor disc planes.

For forward speeds above 60 mph Equation (6.4) can be simplified by letting $\sqrt{V_h^2+v^2} \doteq V_h$, which results in

$$T = 2\pi\rho v V_h\left[(\pi R_e^2 + 2R_e \times Gap) + \left\{A_e - (\pi R_e^2 + 2R_e \times Gap)\right\}\frac{v}{V_h}\right] \qquad 6.5$$

The results of the calculation of induced power for the XH-16 helicopter and the Kármán-Yuan modification are listed below. (Both helicopters have approximately the same P_i.)

$R_e = .96 \times 41$ ft. ; $A_e = 8662$ ft^2 ; Gap = 3.56 ft

$$v = -24.5\, V_h + \frac{\sqrt{(24.5\, V_h)^2 + 66.48\, T}}{33.24} \qquad 6.5a$$

From Equation (6.1) we obtain the induced power P_i;

V_h (mph)	V_h (fps)	v (fps)	P_i (HP)
60	88	15.18	1007
80	117	11.88	788
100	147	9.77	649
120	176	8.42	559
140	206	7.07	470
160	234	6.17	410

6.2 PROFILE POWER

In Reference (13), it has been shown that the profile power in forward flight can be closely approximated by increasing the hovering profile power as a function of the square of the advance ratio μ. Thus the profile power in forward flight becomes

$$P_o = P_{o_{hov}} (1 + \mu^2) \qquad 6.6$$

Since the rotor-tilt angle γ is usually small $\mu \simeq \frac{V}{\Omega R}$ is used in practice.

The results of the calculations of the profile power for the XH-16 and the Karman-Yuan modification are listed below.

	XH-16		Karman-Yuan	
V_h (mph)	$1+\mu^2$	P_o (HP)	$1+\mu^2$	P_o (HP)
0	1.0	742	1.0	137
40	1.0085	748	1.0186	140
60	1.0192	756	1.0418	143
80	1.040	772	1.0746	147
100	1.0532	782	1.1162	153
120	1.0766	799	1.170	160
140	1.1041	820	1.232	169
160	1.1359	843	1.302	179

6.3 PARASITE POWER

The total parasite drag of the whole helicopter is composed of the parasite drag of the helicopter body and that of the rotor. The rotor contribution to the parasite drag may be expressed as follows

$$D_{PR} = \frac{1}{2\pi} \int_0^{2\pi} \int_0^R \frac{1}{2} \rho C_{do} bc (\Omega r + V_h \sin\psi)^2 \sin\psi \, dr \, d\psi$$

$$= \frac{1}{4} C_{do} \rho \sigma \pi R^2 V_h (\Omega R) \qquad \text{per rotor} \qquad 6.7$$

The profile drag coefficient C_{d_o} of a conventional rotor is higher than would result from the drag analysis of the individual blades because of the occurrence of reverse flow areas. We will here also assume a slightly higher C_{d_o} to cover the effect of possible flow spoilage in reverse flow, although that may not be required.

The parasite drag of the helicopter body (except rotors) will be

$$D_{PB} = \frac{1}{2} \rho f V_h^2 \qquad 6.8$$

where the equivalent flat plate area f of the XH-16 helicopter body is as given in Reference (12).

The total parasite power of a tandem rotored helicopter is expressed as follows:

$$P_p = \frac{\rho V^2}{1100} [V_h f + C_{d_o} \sigma \pi R^2 (\Omega R)] \qquad 6.9$$

6.3.1 Calculation of Parasite Power for XH-16 Helicopter

$f = 39.4 \text{ ft}^2$ $\quad \sigma = .0546$ $\quad R = 41 \text{ ft}$

$C_{d_o} = .014$ $\quad \Omega R = 636 \text{ ft/sec}$

$$P_p = 2.16 \times 10^{-6} V_h^2 (39.4 V_h + 2570)$$

The results are summarized in the following table.

V_h (mph)	V_h (fps)	V_h^2 x 2.16x10^{-6}	39.4V_h	P_{pB} (HP)	P_{pR} (HP)	P_p (HP)
40	58.7	.00744	2310	17.2	19.1	36.3
60	88	.01672	3470	58.0	43.0	101
80	117.3	.02975	4620	137.5	76.3	213.8
100	146.7	.0465	5780	269	119.5	388.5
120	176	.0669	6940	464	172	636
140	205	.0908	8090	735	233	968
160	235	.1193	9250	1108	307	1415

6.3.2 Calculation of Parasite Power for Kármán-Yuan Helicopter Modification

$f = 39.4 \text{ ft}^2$ $\sigma = .0546$ $R = 41$ ft

$C_{d_o} = .0085$ $\Omega R = 430$ ft/sec

$$P_p = 2.16 \times 10^{-6} V_h^2 (39.4 V_h + 1055)$$

V_h (mph)	P_{pB} (HP)	P_{pR} (HP)	P_p (HP)
40	17.2	8.0	25
60	58.0	17.7	76
80	137.5	31.3	169
100	269	49	318
120	464	71	535
140	735	96	831
160	1108	126	1234

6.4 SUCTION POWER FOR KÁRMÁN-YUAN HELICOPTER MODIFICATION

The suction power needed in forward flight is actually less than that required in hovering as a result of the small lift coefficient needed in forward flight. However, the suction power used below is assumed to be the same as in hovering, i.e., 350HP for both rotors. A summary of forward flight performance of the two systems is listed below.

V_h (mph)		0	40	60	80	100	120	140	160
V_h (fps)		0	58.7	88	117	147	176	206	234
Piasecki XH-16	P_i Induced	1984	1335	1007	788	649	559	470	410
	P_0 Profile	742	748	756	772	782	799	820	843
	P_p Parasite	0	36	101	214	388	636	968	1415
	P_t Total	2726	2119	1864	1774	1819	1994	2258	2668
Kármán-Yuan	P_i Induced	2020	1335	1007	788	649	559	470	410
	P_0 Profile	137	140	143	147	153	160	169	179
	P_p Parasite	0	25	76	169	318	535	831	1234
	P_s Suction	350	350	350	350	350	350	350	350
	P_t Total	2507	1850	1576	1454	1470	1604	1820	2173
Power Ratio Kármán-Yuan/XH-16		.92	.87	.85	.82	.81	.81	.81	.81

Curves of total power P_t versus speed are plotted in Figure 6.1.

SECTION 7

CALCULATION OF SUCTION POWER REQUIREMENTS

7.1 EXPRESSION FOR SUCTION PRESSURE

A suction pump, or an ejector and venturi tube at the blade tip, is required in the contemplated Karman-Yuan rotor to provide sufficient suction pressure to draw a desired quantity of air mass against the maximum localized negative pressure increments over the wing surface. In addition, the suction provided by the pump must also be sufficient to overcome the pressure drop due to duct friction, loss of momentum, and the pressure drop across the porous skin. In this section the term suction pressure will be used to denote pressure difference between the atmospheric pressure and the absolute pressure, $p_o - p$.

In a uniformly rotating system such as a helicopter rotor an additional component of force in the direction of flow within the duct which is due to the component of the centrifugal acceleration $\Omega^2 r$ in that direction must be added to the above mentioned system. The coriolis acceleration is always at right angles to the direction of the relative flow and hence yields no contribution.

The equation for fluid motion in rectangular ducts can be written as follows:

$$2\rho U_d \frac{dU_d}{dr} b_1 h\, dr + 2\tau_o (h+b_1)\, dr = \frac{d(p_d - p_x)}{dr} b_1 h\, dr + \rho \Omega^2 r\, b_1 h\, dr \qquad 7.1$$

where

U_d = duct velocity at section r,

p_d = suction pressure at section r,

p_x = suction pressure due to lift,

h = the depth of rectangular section duct,

b_1 = the width of rectangular section duct, and

τ_o = duct wall shearing stress.

Integrating Equation (7.1) we obtain an expression for the duct suction pressure at any section r

$$p_d = p_x + p_1 + p_2 - p_3$$

$$= p_x + 2\rho \int U_d \frac{dU_d}{dr} dr + \frac{2\rho}{d} \int C_f U_d^2 dr - \frac{\rho}{2} \Omega^2 r^2 \qquad 7.2$$

where

$$C_f = \frac{\tau_o}{\frac{1}{2}\rho U_d^2}$$

and

$$\frac{d}{4} = \frac{b_1 h}{2(b+h)} \qquad \text{(the hydraulic diameter)}$$

Since the volume flow in the duct is $U_d b_1 h$ and the volume flow into the duct through the porous surface in an element of length dr is $v_s b_1 dr$, the following continuity equation can be established.

$$\frac{d}{dr}(U_d b_1 h)\, dr = V_s b_1 dr \qquad (7.3)$$

For a duct with constant cross-section the duct velocity becomes

$$U_d = \int \frac{V_s}{h} dr = \frac{1}{A} \int Q_s dr \qquad 7.4$$

where Q_s is the suction quantity per unit radial length.

From Section 3 we obtain the following relation.

$$C_Q = \frac{k_r}{\sqrt{R_\ell}} \quad \text{and} \quad R_\ell = \frac{\Omega r c}{\nu}$$

But

$$Q_s = C_Q(\Omega r)c = k_r\sqrt{\Omega r c \nu} \qquad 7.5$$

where k_r is a function of the lift coefficient C_L. Substituting Equation (7.4) into Equation (7.3) yields

$$U_d = \frac{\sqrt{\Omega c \nu}}{A}\int k_r\sqrt{r}\,dr \qquad 7.6$$

If k_r is assumed to be the maximum value, say k, then

$$U_d = \frac{2}{3}\frac{Q_o}{A}\ell x^{3/2} \quad ; \quad x = \frac{r}{\ell} \qquad 7.7$$

where

$$Q_o = k\sqrt{(\Omega R)c\nu} \quad ; \quad \ell = \text{length of duct}$$

From Equation (7.7), the expression for p_1 becomes

$$p_1 = 2\rho\int U_d\frac{dU_d}{dr}dr = \frac{4}{9}\rho\left(\frac{Q_o}{A}\right)^2\ell^2x^3 \qquad 7.8$$

The expression for p_2 becomes

$$p_2 = \frac{2\rho}{d}\int C_f U_d^2\,dr = \frac{8}{9}\left(\frac{Q_o}{A}\right)^2\left(\frac{\ell}{d}\right)\ell^2\int_o^1 C_f x^3\,dx$$

$$= .00311\left(\frac{\ell}{d}\right)\rho\left(\frac{Q_o}{A}\right)^2\ell^2x^4 + .00278\left(\frac{\ell}{d}\right)^{1.32}\rho\left(\frac{Q_o}{A}\right)^{1.68}\ell^{1.68}\left(\frac{\nu}{\ell}\right)^{.32}x^{3.52} \qquad 7.9$$

where

$$C_f = .0014 + .0125\, R_d^{-.32}$$

$$R_d = \frac{U_d d}{\nu} = \frac{3}{2} k \frac{\ell d}{A} \sqrt{R_c}\, X^{3/2}$$

and

$$R_c = \frac{\Omega R_y c}{\nu}$$

The expression for p_x is computed using the maximum value of U at each section in order to be conservative.

$$p_x = p_s - \frac{1}{2}\rho(\Omega R)^2 x^2 \left[1 - \left(\frac{U}{\Omega r}\right)^2\right] \qquad 7.10$$

where p_s is the pressure across the porous skin. The expression for p_3 is

$$p_3 = \frac{1}{2}\rho\Omega^2 r^2 = \frac{1}{2}\rho(\Omega R)^2 x^2 \qquad 7.11$$

7.2 SUCTION DUCTS AND SUCTION QUANTITY

Since the distribution of the lift pressure and suction quantity varies in the chordwise direction it is more economical to use several suction ducts than a single one. However, in the present estimate only a single duct is considered which is assumed to take all the suction quantities at the most adverse condition of wing pressure loading.

The area of the cross section of the duct is assumed to be one-third of the blade cross-section area (0.256 ft^2) and it is located in the rear part of the blade. The calculated values of the perimeter of the duct is 2.235 ft. Thus the hydraulic diameter is

$$d = \frac{4A}{p} = 0.459 \text{ ft.}$$

The suctionnquantity Q_o is obtained from C_Q (page 10);

$$Q_o = 3.33\sqrt{\Omega R c \nu} = 1.333$$

therefore

$$\frac{Q_o}{A} = 5.2$$

In the present calculation a factor of 2.5 is multiplied to the calculated value of Q_o/A

$$\left(\frac{Q_o}{A}\right)_{design} = 13$$

With the above parameters the various pressures which contribute to the duct pressures can be calculated as follows:

$$p_1 = \frac{4}{9}\rho\left(\frac{Q_o}{A}\right)^2 \ell^2 x^3 = 300 x^3$$

$$p_2 = .000311\left(\frac{\ell}{d}\right)\rho\left(\frac{Q_o}{A}\right)^2 \ell^2 x^4 + .00278\left(\frac{\ell}{d}\right)^{1.32}\rho^{1.68}\left(\frac{Q_o}{A}\right)^{1.68}\ell^{1.68}\left(\frac{\nu}{\ell}\right)^{.32} x^{3.52}$$

$$= 18.73 x^4 + 1.774 x^{3.52}$$

$$p_3 = \frac{1}{2}\rho(\Omega R)^2 x^2 = 220 x^2$$

$$p_x = -\frac{1}{2}\rho(\Omega R)^2\left[1-\left(\frac{U}{\Omega r}\right)^2\right]x^2$$

$$= -220\left[1-\left(\frac{U}{\Omega r}\right)^2\right]x^2$$

where $U/\Omega r$ versus x is shown in Figure 7.1. The distribution of C_L is obtained by considering the linear variation of flap angle β versus x so that we can also plot C_L versus $U/\Omega r$ in Figure 7.1.

The computations are summarized in the following tables.

(x)	$(x)^2$	$(x)^3$	$(x)^{3.52}$	$(x)^4$	$1-(U/\Omega r)^2$
0.2	.04	.008	.00343	.0016	- 9.72
0.3	.09	.027	.0144	.0081	- 5.68
0.4	.16	.064	.0395	.0256	- 3.5
0.5	.25	.125	.0895	.0625	- 2.33
0.6	.36	.216	.165	.1296	- 1.56
0.8	.64	.512	.456	.410	- .99
0.96	.922	.885	.866	.850	- .69

(x)	p_x	p_1	$-p_3$	p_d
0.2	85.2	2.4	- 8.8	78.8
0.3	112.5	8.1	- 19.8	100.8
0.4	123	19.2	- 35.2	107
0.5	128	37.5	- 55	110.5
0.6	124	64.8	- 79.2	109.6
0.8	125	154	- 141	138
0.96	140	265	- 203	202

p_2 is negligible

The calculated maximum duct suction pressure at the tip is $202\#/ft^2$. The designed maximum suction pressure in the duct is assumed to be $300\ \#/ft^2$ in order to be conservative. The required suction power for one blade is

$$P_s = \frac{p_{d\,max}}{550} \int_{.2}^{.96} Q_s \ell \, dx \qquad ; \qquad Q_s = Q_o \sqrt{x}$$

$$P_s = \frac{(300)(41)}{550} Q_o \int_{.2}^{.96} \sqrt{x}\, dx = \frac{(300)(41)}{550} (13 \times .256) \frac{2}{3} \left[x^{3/2} \right]_{.2}^{.96}$$

$$= 42 \text{ HP}$$

Total suction for one rotor is 126 HP, ($3 \times P_s$ for the three blades).

$$U_{d(tip)} = \frac{2}{3} \frac{Q_o}{A} \ell x^{3/2} = \frac{2}{3} (13)(41)(.936) = 331 \text{ ft/sec.}$$

$$Q_T = \ell \int_{.2}^{.96} Q_s \, dx = (41)(13 \times .256) \frac{2}{3} \left[x^{3/2} \right]_{.2}^{.96} = 85 \text{ cu. ft./sec.}$$

If the weight of the blower is estimated at 4 pounds per horsepower and the duct equipment is assumed to be 100 pounds per rotor the total weight of the suction system is about 600 pounds per rotor. For the XH-16 helicopter the power loading is about 13 pounds per horsepower. There will be required an additional power of 46 horsepower per rotor due to the weight of suction equipment. Therefore the total suction power required is about 175 horsepower per rotor for the maximum estimate.

This estimate can be reduced considerably if a tip venturi or tip ejector is used to draw the boundary layer in the outer part of the blades and a pump system is used to draw the boundary layer in the inner portion of the blades.

7.3 REVERSE FLOW CHARACTERISTICS

One of the limiting factors in performance of orthodox helicopters is that resulting from the loss of lift in the region of reverse flow when a helicopter is in forward flight. It is believed that this loss of lift and limiting effect on performance can be avoided to a great extent by application of the Kármán-Yuan system.

If an additional flap is placed along the dividing streamline in the vicinity of the leading edge of the oval shaped airfoil, approximately the same lift would be produced as there would be without the leading edge flap. Now, if the flow over the airfoil is reversed, approximately the same lift would again be obtained, for, aside from separation, it can be shown that the pattern of streamlines and pressure distribution is independent of the sign of the velocity of flow. The only requirement is that in addition to the suction at the trailing edge, suction must be applied at the leading edge in that region where reverse flow would be experienced. For this reason, the Kármán-Yuan rotor blades would not experience loss of lift in the reverse flow region. Furthermore, the higher blade lift coefficient obtained at the inner portion of the blade would result in a favorable spanwise lift distribution.

SECTION 8

AEROELASTIC CHARACTERISTICS OF THE KÁRMÁN-YUAN ROTOR

8.1 DIVERGENCE AND AILERON REVERSAL

Using the procedures of Reference (8) the steady lift L and moment M_o with respect to the center of an elliptic airfoil section (Figure 8.1) is

8.1

$$L = 2\pi\rho U_o^2 (a+b) \sin(\alpha+\beta)$$

$$M_o = \tfrac{1}{2}\pi\rho U_o^2 (a^2-b^2) \sin 2\alpha$$

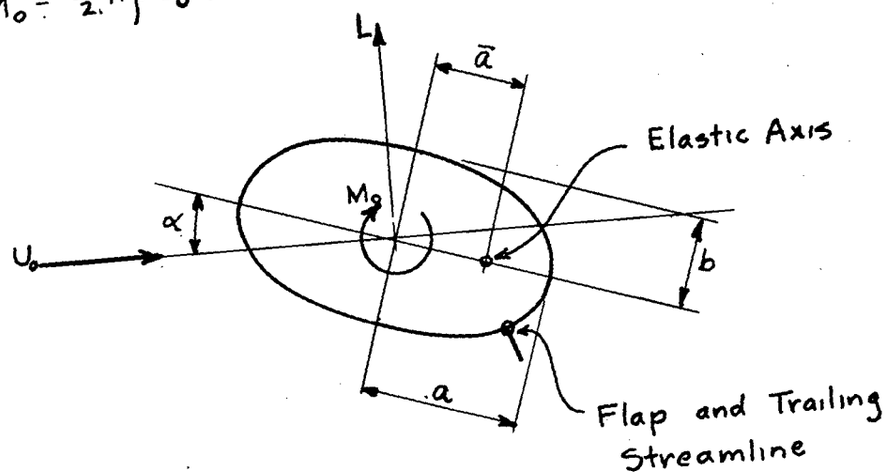

Figure 8.1

where $C_L = 2\pi(1 + b/a) \sin\beta$ (defined with the assumption that $\alpha = 0$).

The total aerodynamic moment M_a about the elastic axis of the section is

$$M_a = M_o + \bar{a} L \cos\alpha = \pi\rho U_o^2 (a^2-b^2)\left[\frac{\sin 2\alpha}{2} + \frac{2\bar{a}}{a-b} \sin(\alpha+\beta)\cos\alpha\right] \qquad 8.2$$

In the analysis of the divergence of a rotor blade, the torsional resisting moment $M_\alpha(r)$ developed by the blade as a result of a rotation α, is a rather complicated function of the radial distance r along the blade. Nevertheless we may define a section torsional stiffness $C_\alpha(r)$ such that

$$M_\alpha(r) = \alpha C_\alpha(r) \qquad 8.3$$

Equating the total aerodynamic moment M_a at section r with the resisting moment M_α, we obtain

$$\pi\rho U_o^2 (a^2-b^2)\left[\frac{\sin 2\alpha}{2} + \frac{2\bar{a}}{a-b}\sin(\alpha+\beta)\cos\alpha\right] = \alpha C_\alpha$$

or

$$U_o^2 = \frac{C_\alpha}{\pi\rho(a^2-b^2)\left[\frac{\sin 2\alpha}{2\alpha} + \frac{2\bar{a}\sin(\alpha+\beta)\cos\alpha}{(a-b)\alpha}\right]} \qquad 8.4$$

If the denominator of Equation (8.4) is zero or negative for every section of the rotor blade, then the divergence velocity for the entire blade must become infinite or imaginary. The divergence criterion can be expressed

$$\frac{\sin 2\alpha}{2\alpha} + \frac{2\bar{a}}{a-b}\frac{\sin(\alpha+\beta)\cos\alpha}{\alpha} \leq 0$$

or

$$\bar{a} \leq -\frac{a-b}{2}\frac{\sin\alpha}{\sin(\alpha+\beta)} = \bar{a}_L \qquad 8.5$$

From Equations (8.1) and (8.2) it is seen that the right hand side of the inequality (8.5) is the location of the center of pressure $\bar{a}_L$, so that the divergence criterion (8.5) requires the elastic axis to be located upstream of the center of pressure in order to preclude the possibility of divergence at any speed.

If it is assumed that α' is a small variation from the initially zero angle of attack, the Equation (8.5) can be written

$$\bar{a} \leq - \frac{a-b}{2} \frac{\alpha'}{\sin \beta} \qquad 8.6$$

We may conclude that for zero initial angle of attack, (center of pressure at the center of the airfoil), location of the elastic axis at or upstream of the center of the airfoil insures an infinite divergence speed.

The above criterion for divergence, which involves the location of the center of pressure of the total lift on the airfoil is inadequate in discussing stability of the airfoil with regard to perturbation lift forces. The location $x = \bar{a}_\Delta$ of these perturbation forces is

$$\bar{a}_\Delta = - \frac{dM}{dL} = - \frac{a-b}{2} \frac{\cos 2\alpha}{\cos (2\alpha+\beta)} \qquad 8.7$$

For initial angle of attack equal to zero, this becomes

$$\bar{a}_\Delta = - \frac{a-b}{2 \cos \beta} \qquad 8.8$$

It should be noted that the perturbation may be caused by a change of angle of attack α , but not by a change of flap angle β , since $dM/d\beta$ is zero.

The perturbation center of pressure $\bar{a}_\Delta$ is of importance in unsteady aerodynamic problems and will be further considered in the discussion of flutter.

Comparing steady and perturbation centers of pressure $\bar{a}_L$ and $\bar{a}_\Delta$, it is seen that the letter is in general well upstream of the former, $\bar{a}_\Delta$ lying in the vicinity of the quarter chord in the case of an elliptical profile.

Since control reversal involves the change in pitching moment about the elastic axis resulting from change in control position, it is obvious from Equation (8.1) that although a change in β will change the lift, it will not effect the pitching moment about the midchord. For elastic axes slightly forward of the midchord and with sufficient torsional rigidity, it appears that the problem of aileron reversal should not cause any difficulty.

8.2 AERODYNAMIC DERIVATIVES FOR FLUTTER OF AN ELLIPTICAL AIRFOIL

Using the procedures and notations of Reference (9), the complex potential associated with the translation and rotation without circulation of an elliptic cylinder with semi-axes a and b, which is instantaneously fixed at the origin of, and oriented parallel to a coordinate system x,y, is

$$w = \frac{U_1}{\zeta}\left(A^2 - \frac{c_0^2}{4}\right) + \frac{iV_1}{\zeta}\left(A^2 + \frac{c_0^2}{4}\right) + \frac{i\Omega c_0^2 A^2}{4\zeta^2} \qquad 8.9$$

where

$$A = \frac{a+b}{2}$$
$$c_0^2 = a^2 - b^2 \qquad 8.10$$

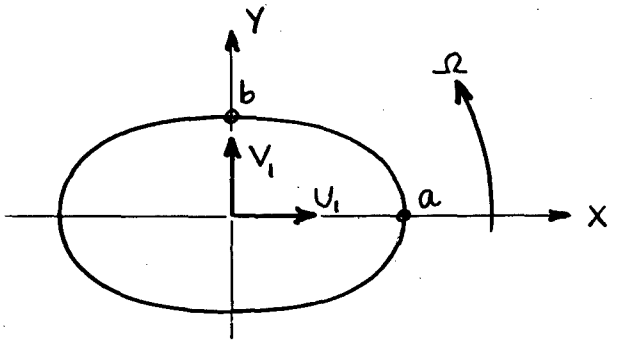

Figure 8.2

U_1 and V_1 are the velocity components in the positive x and y directions. We define the complex variables

$$z = x + iy$$
$$\zeta = \xi + i\eta \qquad 8.11$$

where

$$\zeta = z + \frac{c_o^2}{4z} \qquad 8.12$$

Equation (8.12) is the transformation equation relating the elliptic contour in the z plane with the circular contour of radius A in the ζ plane, $\zeta = A\, e^{i\theta}$.

Since this is a linear theory, we can separate the forces and moments on the elliptic airfoil into non-circulatory and circulatory parts and then superpose them. The former is obtained exactly by use of Lagrange's Equation for moving coordinates (Reference (9)) whereas the latter is obtained approximately by assuming proportionality with certain terms of the Theodorsen theory.

To obtain the kinetic energy without circulation for use in Lagrange's Equation we obtain the potential function and the stream function on the contour of the cylinder from Equation (8.9)

$$\varphi_{onc} = U_1 b \cos\theta + V_1 a \sin\theta + \frac{\Omega c_0^2}{4} \sin 2\theta \qquad 8.13a$$

or

$$\varphi_{onc} = U_1 b \frac{x}{a} + V_1 a \sqrt{1 - \frac{x^2}{a^2}} + \frac{\Omega c_0^2 x}{2a} \sqrt{1 - \frac{x^2}{a^2}} \qquad 8.13b$$

and

$$\psi_{onc} = - U_1 b \sin\theta + V_1 a \cos\theta + \frac{\Omega c_0^2}{4} \cos 2\theta \qquad 8.14$$

The kinetic energy is

$$T = - \frac{\rho}{2} \oint \varphi \, d\psi = \frac{\pi\rho}{2} \left[U_1^2 b^2 + V_1^2 a^2 + \frac{\Omega^2 c_0^4}{8} \right] \qquad 8.15$$

The upward force $\vec{F}$ and counterclockwise moment $\vec{L}$ exerted by the liquid on the moving cylinder is given by

$$- \frac{d}{dt} \frac{\partial T}{\partial \vec{q}} - \vec{\Omega} \times \frac{\partial T}{\partial \vec{q}} = \vec{F} \qquad 8.16$$

$$- \frac{d}{dt} \frac{\partial T}{\partial \vec{\Omega}} - \vec{\Omega} \times \frac{\partial T}{\partial \vec{\Omega}} - \vec{q} \times \frac{\partial T}{\partial \vec{q}} = \vec{L}$$

where

$$\vec{q} = U_1 \hat{i} + V_1 \hat{j} \qquad 8.17$$

$$\vec{\Omega} = \Omega \hat{k}$$

and

$$\frac{\partial T}{\partial \vec{q}} = \hat{i}\frac{\partial T}{\partial U_1} + \hat{j}\frac{\partial T}{\partial V_1} = \pi\rho\left[b^2 U_1 \hat{i} + a^2 V_1 \hat{j}\right]$$

$$\frac{\partial T}{\partial \vec{\Omega}} = \hat{k}\frac{\partial T}{\partial \Omega} = \pi\rho\,\hat{k}\left[\frac{\Omega c_0^4}{8}\right] \qquad 8.18$$

$\hat{i}$ and $\hat{j}$ indicate unit vectors in the instantaneous x and y directions. We obtain

$$\vec{F} = -\pi\rho\left[\hat{i}\left(b^2\dot{U}_1 - a^2\Omega V_1\right) + \hat{j}\left(a^2\dot{V}_1 + b^2\Omega U_1\right)\right]$$

$$\vec{L} = -\pi\rho\,\hat{k}\left[\frac{\dot{\Omega}c_0^4}{8} + c_0^2 U_1 V_1\right] \qquad 8.19$$

In order to observe the usual sign conventions for a cylinder moving in the negative direction relative to the fluid, vertical deflection positive downward, lift positive downward, angular rotation and moment positive nose upward, we make the following change of coordinates

$$\Omega = -\dot{\alpha}$$

$$U_1 = -U_0$$

$$V_1 = -\left(\dot{h} + U_0\alpha\right) \qquad 8.20$$

$$L = -M_{nco}$$

$$\vec{F}\cdot\hat{j} = -P_{nco}$$

We then obtain

$$P_{nco} = -\pi\rho\left[a^2(\ddot{h} + U_o\dot{\alpha}) - b^2 U_o \dot{\alpha}\right]$$

$$M_{nco} = -\pi\rho\left[\frac{c_o^4\ddot{\alpha}}{8} - c_o^2 U_o(\dot{h} + U_o\alpha)\right] \qquad 8.21$$

The non-circulatory force P_{NC} for rotation of the airfoil about an elastic axis $x = \bar{a}$ is obtained by replacing h by $h - \bar{a}\alpha$, so that

$$P_{nc} = -\pi\rho a^2\left[(\ddot{h} - \bar{a}\ddot{\alpha}) + \frac{c_o^2}{a^2} U_o \dot{\alpha}\right] \qquad 8.22$$

Similarly, the non-circulatory moment about the elastic axis $x = \bar{a}$ is

$$M_{nc} = M_{nco}(h - \bar{a}\alpha, \alpha) - \bar{a} P_{nc}$$

$$= -\pi\rho a^2\left[a^2\ddot{\alpha}\left(\frac{c_o^4}{8a^4} + \frac{\bar{a}^2}{a^2}\right) - U_o\dot{h}\frac{c_o^2}{a^2} - \bar{a}\ddot{h}\right] \qquad 8.23$$

The above expressions are in agreement with Theodorsen's non-circulatory forces and moments for the case b = 0, a flat plate.

For the circulatory forces and moments due to the wake we assume that the wake vorticity is transported by the stream so that it possesses a constant velocity U_o relative to the airfoil. We further assume that the induced flow about the airfoil is the same as that about a flat plate of chord 2a.

We now introduce a Kutta condition for the purpose of establishing the strength of the total wake vorticity. We see that the unsteady component of velocity at any point of the ellipse can be expressed in the form

$$\frac{\left(\dot{h}+U_0\alpha\right)\frac{x}{a}+\left[\frac{c_0^2}{a}\left(\frac{x^2}{a^2}-\frac{1}{2}\right)-\bar{a}\right]\dot{\alpha}}{\sqrt{1-\frac{c_0^2}{a^2}\frac{x^2}{a^2}}} \qquad 8.24$$

The velocity at a point x of the ellipse due to the total vorticity is of the form

$$\int \frac{f_1(s,x)\,U(s)\,ds}{\sqrt{1-\frac{c_0^2}{a^2}\frac{x^2}{a^2}}} \qquad 8.25$$

where s is the element of length of the trailing streamline measured from the separation point. By equating expressions (8.24) and (8.25) at the point of the ellipse $x = x_0 = a\cos\beta$ we obtain the relationship

$$Q = \left(\dot{h}+U_0\alpha\right) + \frac{\frac{c_0^2}{a}\left(\cos^2\beta-\frac{1}{2}\right)-\bar{a}}{\cos\beta}\dot{\alpha}$$

$$= \frac{1}{2\pi}\int_0^\infty f_1(s,\beta)\,U(s)\,ds \qquad 8.26$$

The moment about the reference point $\bar{a}$ due to the vorticity in the wake is expressible in the form

$$M_r = \rho U_0 c_0^2 \int_0^\infty f_2(s,\beta)\,U(s)\,ds$$

$$= 2\pi\rho\,U_0\,c_0^2\,\frac{\int_0^\infty f_2(s,\beta)\,U(s)\,ds}{\int_0^\infty f_1(s,\beta)\,U(s)\,ds}\,Q$$

or

$$M_r = 2\pi\rho U_o c^2 B(k,\beta) Q \qquad 8.27$$

where $B(k,\beta)$ is the ratio of the two infinite integrals as written above.

Examining the non-circulatory moment, Equation (8.23) we see that it can be written in the form

$$M_{nc} = \pi\rho c_o^2 U_o (\dot{h} + U_o\alpha) + \pi\rho a^2 \left[\bar{a}\ddot{h} - a^2\ddot{\alpha}\left(\frac{c_o^4}{8a^4} + \frac{\bar{a}^2}{a^2}\right)\right]$$

$$= \pi\rho c_o^2 U_o \left[Q - \left(\frac{c_o^2}{a}\left(\cos^2\beta - \frac{1}{2}\right) - \bar{a}\right)\frac{\dot{\alpha}}{\cos\beta}\right]$$

$$+ \pi\rho a^2 \left[\bar{a}\ddot{h} - a^2\ddot{\alpha}\left(\frac{c_o^4}{8a^4} + \frac{\bar{a}^2}{a^2}\right)\right] \qquad 8.28$$

Adding Equations (8.27) and (8.28) we see that the total moment M_α is written

$$M_\alpha = -\pi\rho a^2 \left[\left(\frac{c_o^2}{a}\left(\cos^2\beta - \frac{1}{2}\right) - \bar{a}\right) U_o\dot{\alpha}\frac{c_o^2}{a^2\cos\beta} + a^2\ddot{\alpha}\left(\frac{c_o^4}{8a^4} + \frac{\bar{a}^2}{a^2}\right)\right.$$

$$\left. - \bar{a}\ddot{h}\right] + 2\pi\rho U_o c_o^2 \left[\bar{l}\,\bar{C}_M(\beta,k)\,Q\right] \qquad 8.29$$

where $a\bar{l}$ will be seen to be the location of the center of pressure, and $\bar{C}_M(\beta,k)$ is a new function of β and k to replace $B(\beta,k)$.

The most general possible form of $\bar{l}$, consistent with linear theory, can be written

$$\bar{l} = l_o + l_1 h + l_2 \alpha$$

But $\bar{l}Q$ to be linear requires that

$$\bar{l} Q = l_o Q$$

If we go to the limit $\omega \rightarrow 0$, we find that steady M_α is

$$M_\alpha \rightarrow 2\pi \rho U_o^2 \alpha \left[l_o \bar{C}_M(\beta, 0) \right] c_o^2 \qquad 8.30$$

From Equation (8.2) of the previous section, we find that the "steady" moment due to small perturbations of the angle of attack from an initially zero value is

$$M_\alpha = \alpha \left[\frac{\partial M_a}{\partial \alpha} \right]_{\alpha_o = 0} = 2\pi \rho U_o^2 a^2 \left(1 + \frac{b}{a} \right) \cos\beta \left(\frac{\bar{a}}{a} + \frac{1 - \frac{b}{a}}{2\cos\beta} \right) \alpha$$

so that

$$c_o^2 l_o \bar{C}_M(\beta, 0) = a^2 \cos\beta \left(1 + \frac{b}{a} \right) \left(\frac{\bar{a}}{a} + \frac{1 - b/a}{2\cos\beta} \right) \qquad 8.31$$

Substituting the value of l_o obtained from Equation (8.31) into (8.29), we obtain

$$M_\alpha = -\pi \rho a^2 \left[a^2 \ddot{\alpha} \left(\frac{c_o^4}{8a^4} + \frac{\bar{a}^2}{a^2} \right) - \bar{a} \ddot{h} \right] - \pi \rho c^2 U_o \dot{\alpha} \frac{\frac{c_o^2}{a} (\cos^2\beta - \frac{1}{2}) - \bar{a}}{\cos\beta}$$

$$+ 2\pi \rho U_o a^2 \cos\beta \left(1 + b/a \right) \left[\frac{\bar{a}}{a} + \frac{1 - b/a}{2\cos\beta} \right] \frac{\bar{C}_M(\beta, k)}{\bar{C}_M(\beta, 0)} Q \qquad 8.32$$

The circulatory lift is obtained in a similar manner. Thus

$$P_\Gamma = -\rho U_0 a \int_0^\infty f_3(s,\beta)\, U(s)\, ds$$

$$= -2\pi\rho U_0 a\, Q\, \bar{C}_p(\beta,k) \qquad 8.33$$

where

$$\bar{C}_p(\beta,k) = \frac{\int_0^\infty f_3(s,\beta)\, U(s)\, ds}{\int_0^\infty f_1(s,\beta)\, U(s)\, ds} \qquad 8.34$$

Then, adding Equations (8.22) and (8.33)

$$P = -\pi\rho a^2 \left[(\ddot{h} + \bar{a}\ddot{\alpha}) + \frac{c_0^2}{a^2} U_0 \dot{\alpha} \right]$$

$$- 2\pi\rho U_0 a\, \bar{C}_p(\beta,k)\, Q \qquad 8.35$$

When β and b are zero Equations (8.32) and (8.35) reduce to Theodorsen's expressions for the flat plate.

From Equation (8.32) we see that the first term in the bracket is conservative and does not contribute to energy exchange whereas the second and third terms are unconservative and contribute to the mechanism of flutter. The second term vanishes when

$$\bar{a} = \frac{c_0^2}{a}\left(\cos^2\beta - \frac{1}{2}\right) \qquad 8.36$$

and the third term, when

$$\bar{a} = \frac{b-a}{2\cos\beta} \qquad 8.37$$

For the flat plate, $\beta = 0$ and $c_o = a$, Equation (8.36) corresponds to the three-quarter chord and Equation (8.37) to the quarter chord. In the case of a thin ellipse, and β small, there should not be much change in these locations. Since the criterion for precluding flutter is associated with the quarter chord location, it appears that the same will be true for the thin ellipse.

In the case of orthodox airfoils incorporating control surfaces such as ailerons, control reversal inits simplest aspect may be thought of as arising basically from the added load due to control surface movement acting in the vicinity of the midchord, while added load due to incidence changes acts near the quarter chord. Because of the latter centroid of loading it is usual practice to locate the elastic axis of an orthodox system in the vicinity of the quarter chord. We see then that the use of a flap in the usual airfoil results in the loss of control surface effectiveness. Any helicopter blade, incorporating the usual design would experience both loss of control effectiveness and undesirable vibration in forward flight. Since the Thwaites airfoil incorporates a small chord flap located in a region of comparatively small loadings and induces lift by change in angle β so that there results no shift of center of pressure, the control forces and steady forces act at the same location, thereby allowing for increases in lift or control forces without loss of control effectiveness. To accomplish this it is necessary only to locate the elastic axis in the vicinity of the midchord. An alternative and possibly more practical means of varying lift forces on the Thwaites airfoil would be to incorporate a flap which is hinged at a fixed point on the ellipse. The cyclic variation of force could be obtained by oscillating the flap about its root hinge, relative to a static position. Although this would require a somewhat larger flap chord, it is believed that the resulting load would, as in the case of an orthodox flap, still act in the vicinity of the midchord.

Although, according to previous arguments the Thwaites system appears to have good characteristics from the standpoint of reversal and divergence, its characteristics with reference to flutter are not as clear cut. Assuming that an elliptical airfoil is used, it appears that since the static center of pressure is at the midchord and the perturbation center of pressure, associated with flutter is in the vicinity of the quarter chord, that an obvious difficulty arises. It is believed that by incorporating large torsional rigidity while maintaining low flexural rigidity, a sufficiently high flutter speed could be obtained, However, it should be noted that the elliptical profile has been the basis of the present analysis only for purposes of convenience. It is believed that other profiles of an oval shape, while maintaining-the features described in this report would allow for the two centers of pressure to be closer together.

LIST OF REFERENCES

(1) Aerojet Report No. 509, Low Speed Flight Research Program Analysis Report, Series II, Wind Tunnel Tests (1951)

(2) Thwaites, B., The Production of Lift Independently of Incidence, R & M 2611 (1952)

(3) Thwaites, B., On the Design of the Airfoil for which the Lift is Independent of Incidence, R & M 2612 (1952)

(4) United Aircraft Corporation, Analysis of Two-Dimensional Tunnel Tests of a Wing Employing Pressure Slots and Flaps, U.A.C. Report No. R-278, East Hartford, Conn., October 1942

(5) United Aircraft Corporation, Effect of Trailing Edge Suction and Pressure Slots, U.A.C. Report No. R-95374-3, East Hartford, Conn., February 1951

(6) United Aircraft Corporation, Comparison of Three Wings of Different Airfoil Section Employing Pressure Slots and Flaps, U.A.C. Report No. R-278-B, East Hartford, Conn., January 1944

(7) United Aircraft Corporation, Proposal, U.A.C. Report No. P-15174-3

(8) Yuan, S. W., Separation Prevention by Boundary-Layer Suction for Bodies of Arbitrary Shape, Aerojet Report No. 517 (Special) (1951)

(9) Milne-Thomson, L. M., Theoretical Hydrodynamics, MacMillan & Company Ltd., London (1950)

(10) Bussman, K. and Mung, H., "Über die Stabilität der laminaren Reibungschicht mit Absaugang, Jahrbuch 1942 der Deutschen Luftfahrtforschung, p. 36 (German)

(11) Tetervin, N., A Method for Rapid Estimation of Turbulent Boundary Layer Thickness for Calculating Profile Drag, NACA ACR Report No. L4G14 (1944)

(12) Sloan, L.H., Harris, R.J., and Ulrich, K.W., Part I - Performance Data Report, Piasecki Helicopter Corporation Report No. 15-A-14, June 1950

(13) Wald, Quentin, A Method for Rapid Estimation of Helicopter Performance, Journal of Aeronautical Sciences, April 1943

(14) Stepniewski, W.Z., Introduction to Helicopter Aerodynamics, Rotorcraft Publishing Committee, Norton, Pa. (1950)

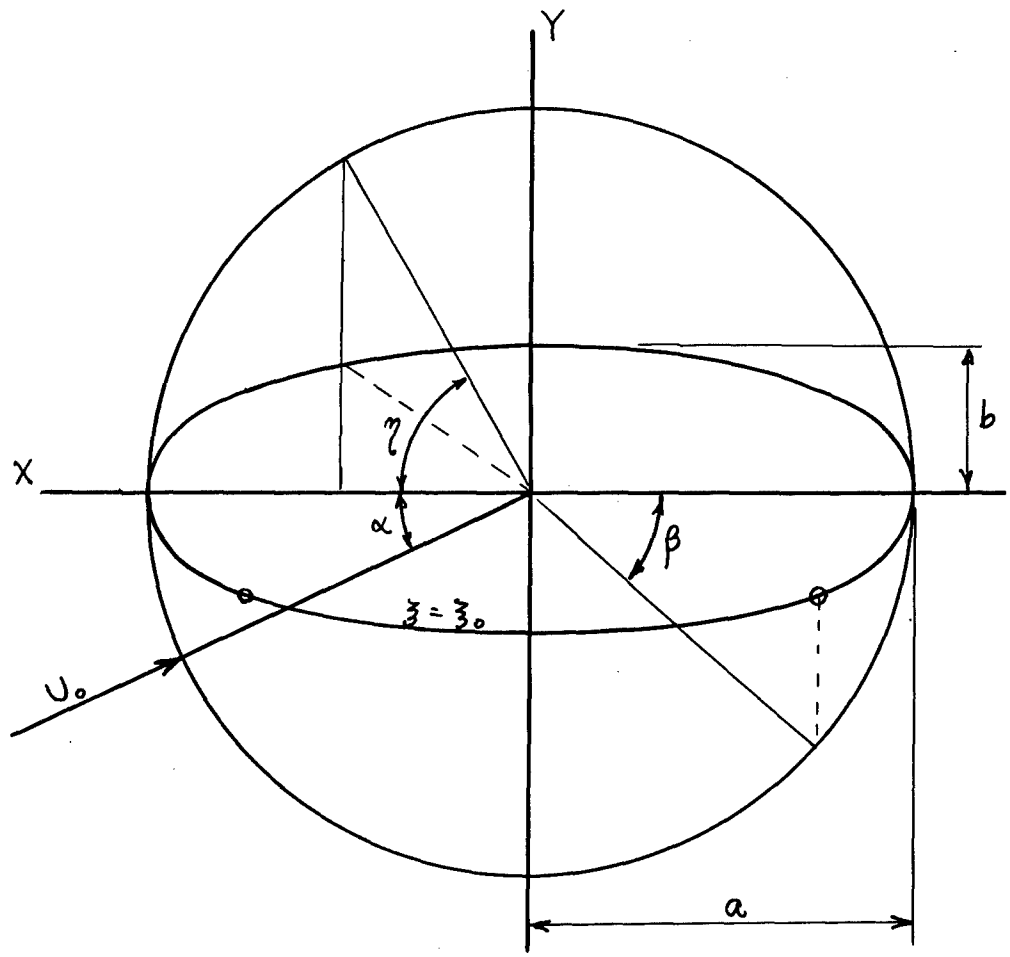

$$Z = X + iY = a\cos\eta + ib\sin\eta \quad \text{(on ellipse)}$$

⊙ - Stagnation Points

Figure 2.1 Elliptic Coordinates

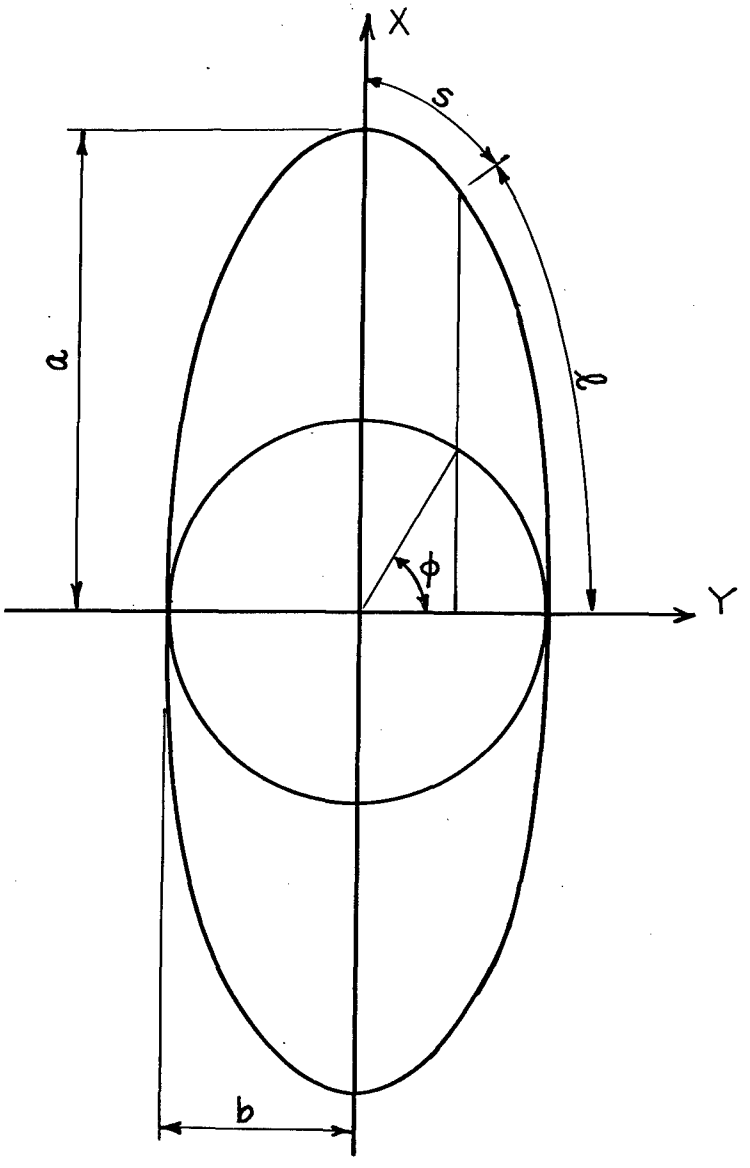

$$\frac{\ell}{a} = \int_0^{\phi} \sqrt{1 - k^2 \sin^2 \varphi}\, d\varphi$$

$$k^2 = 1 - \frac{b^2}{a^2} \quad ; \quad a > b$$

$$\eta = 90° - \phi$$

Figure 2.2 Length of Arc of Ellipse

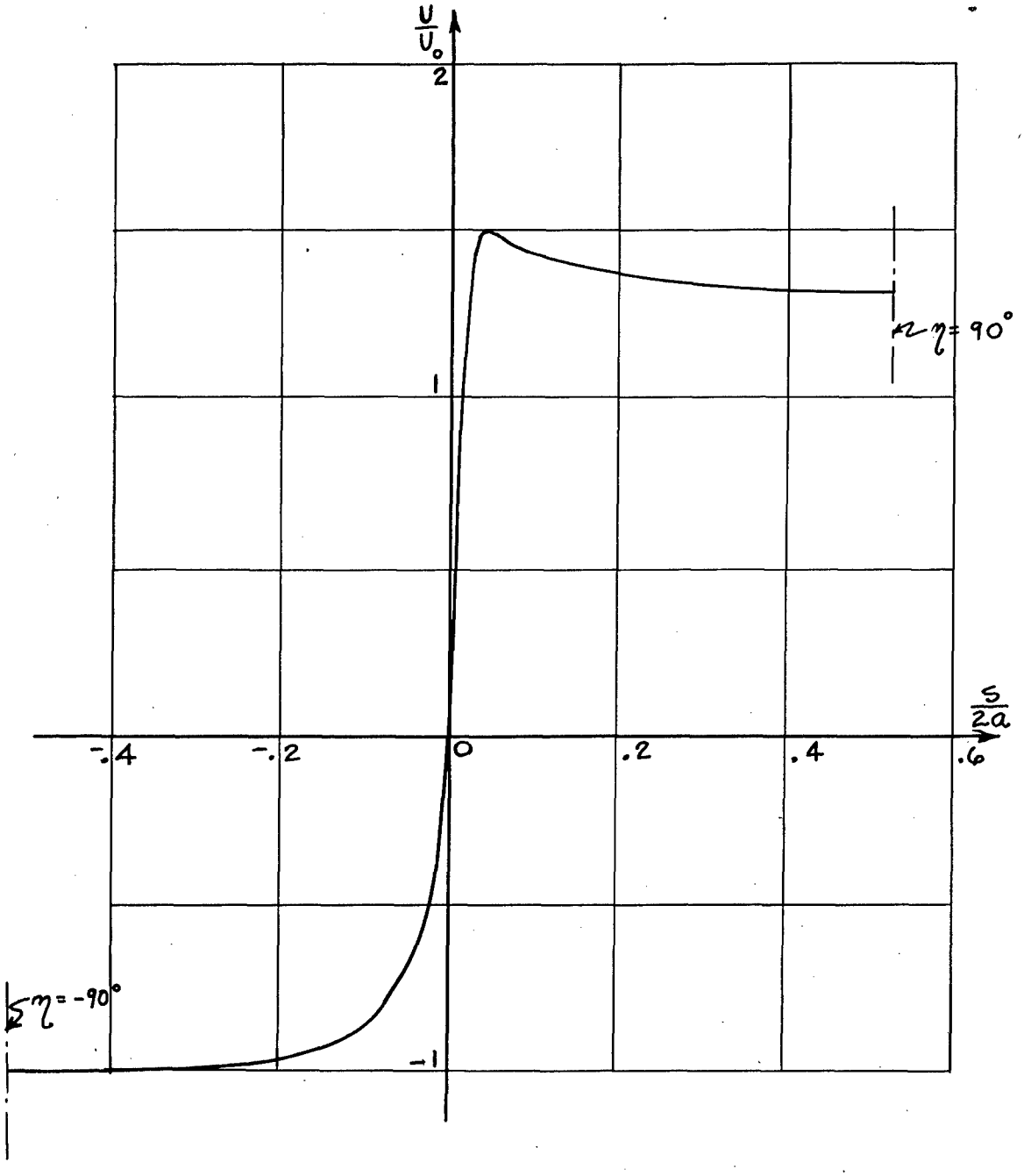

Figure 2.3 Velocity Distribution, $C_L = 1$

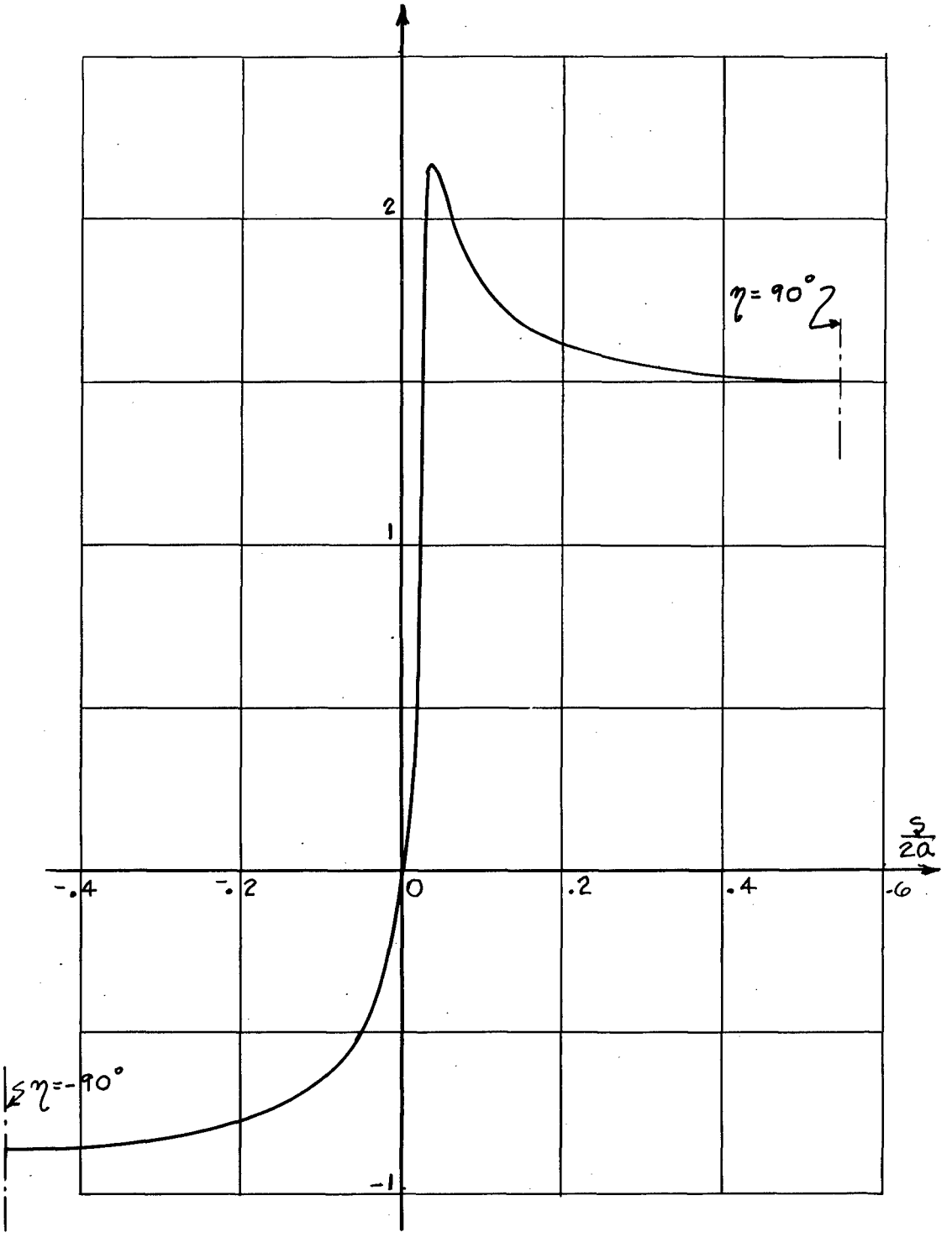

Figure 2.4 Velocity Distribution, $C_L = 2$

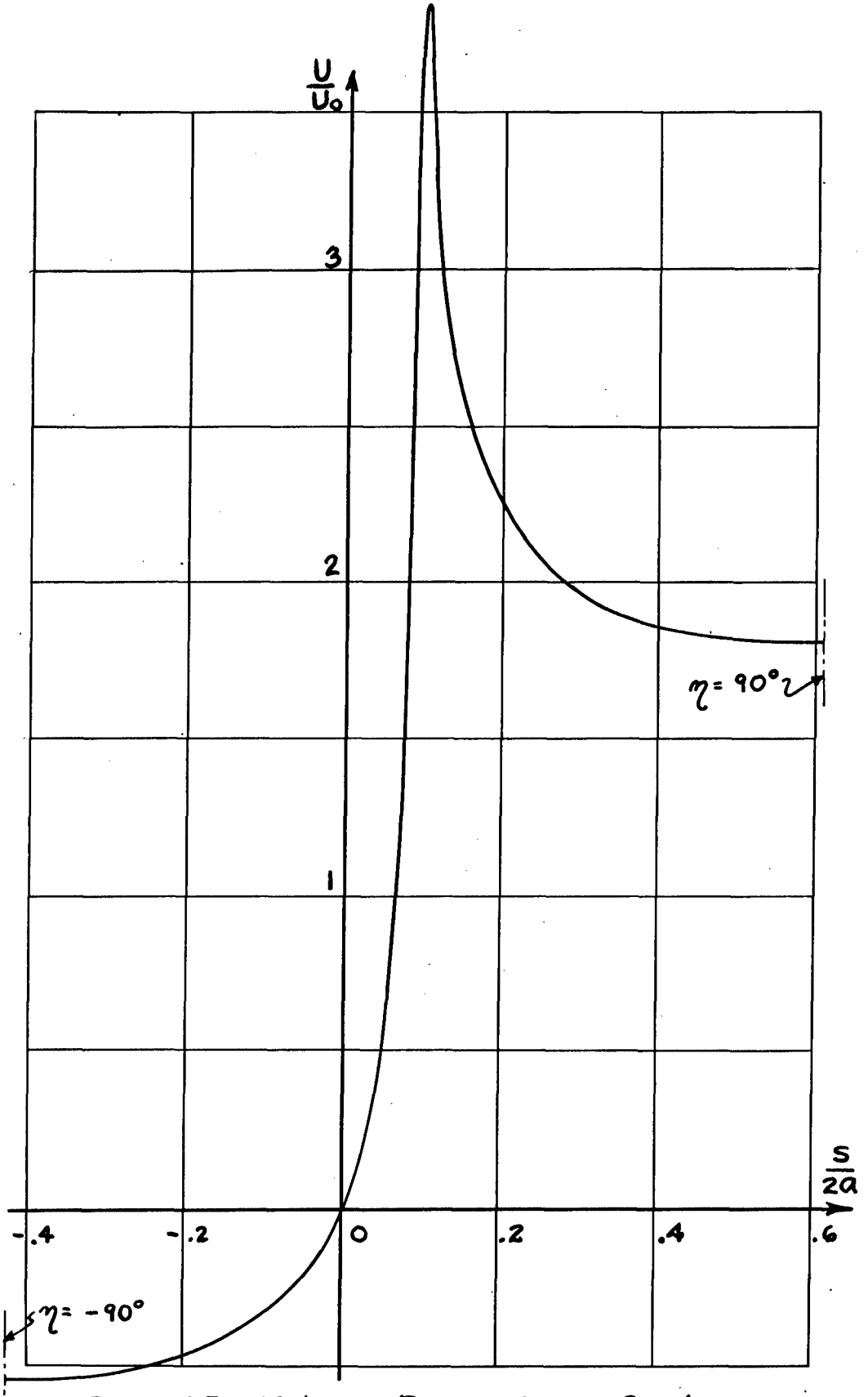

Figure 2.5- Velocity Distribution , $C_L = 4$

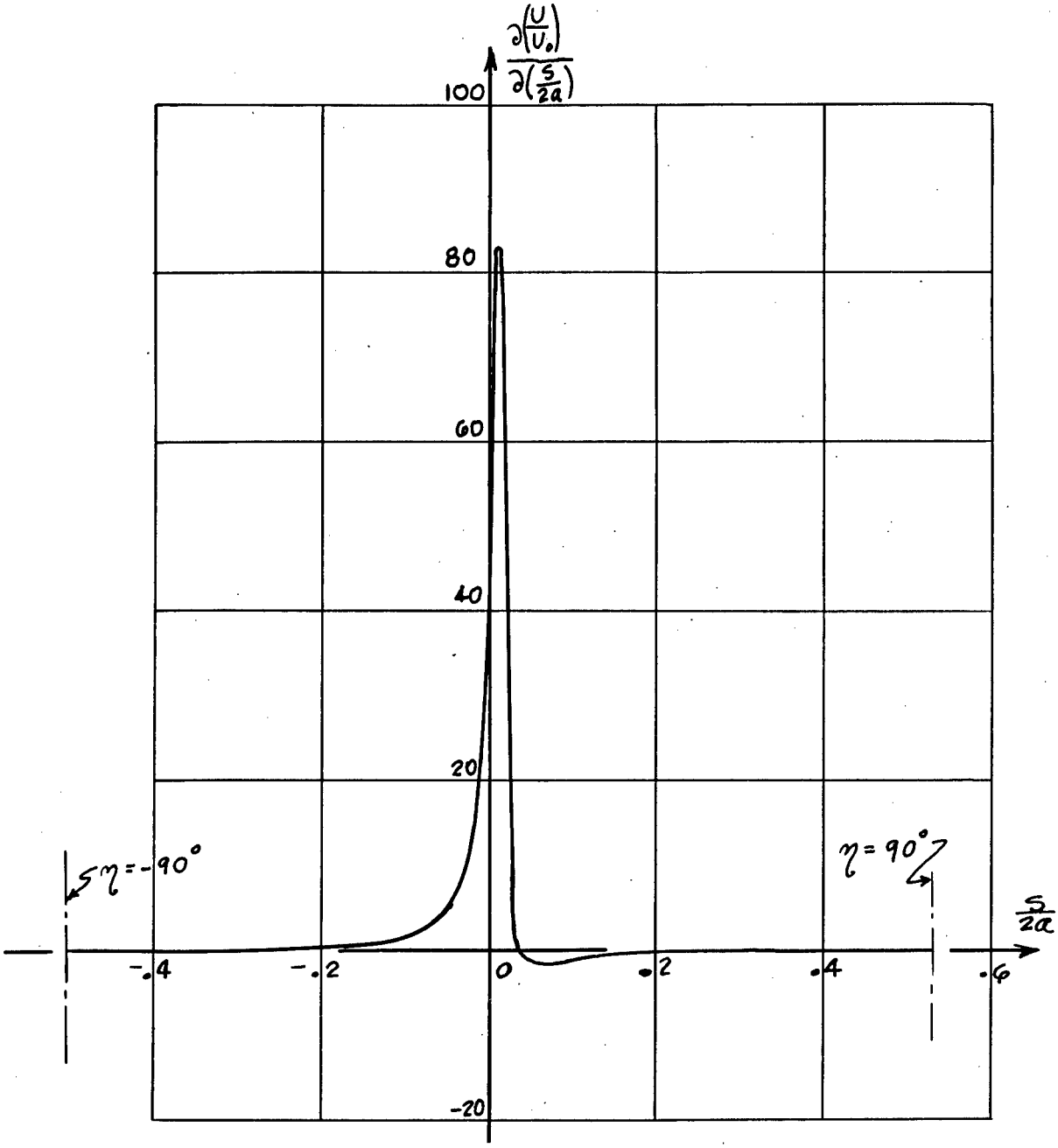

Figure 2.6 Velocity Gradient, $C_L = 1$

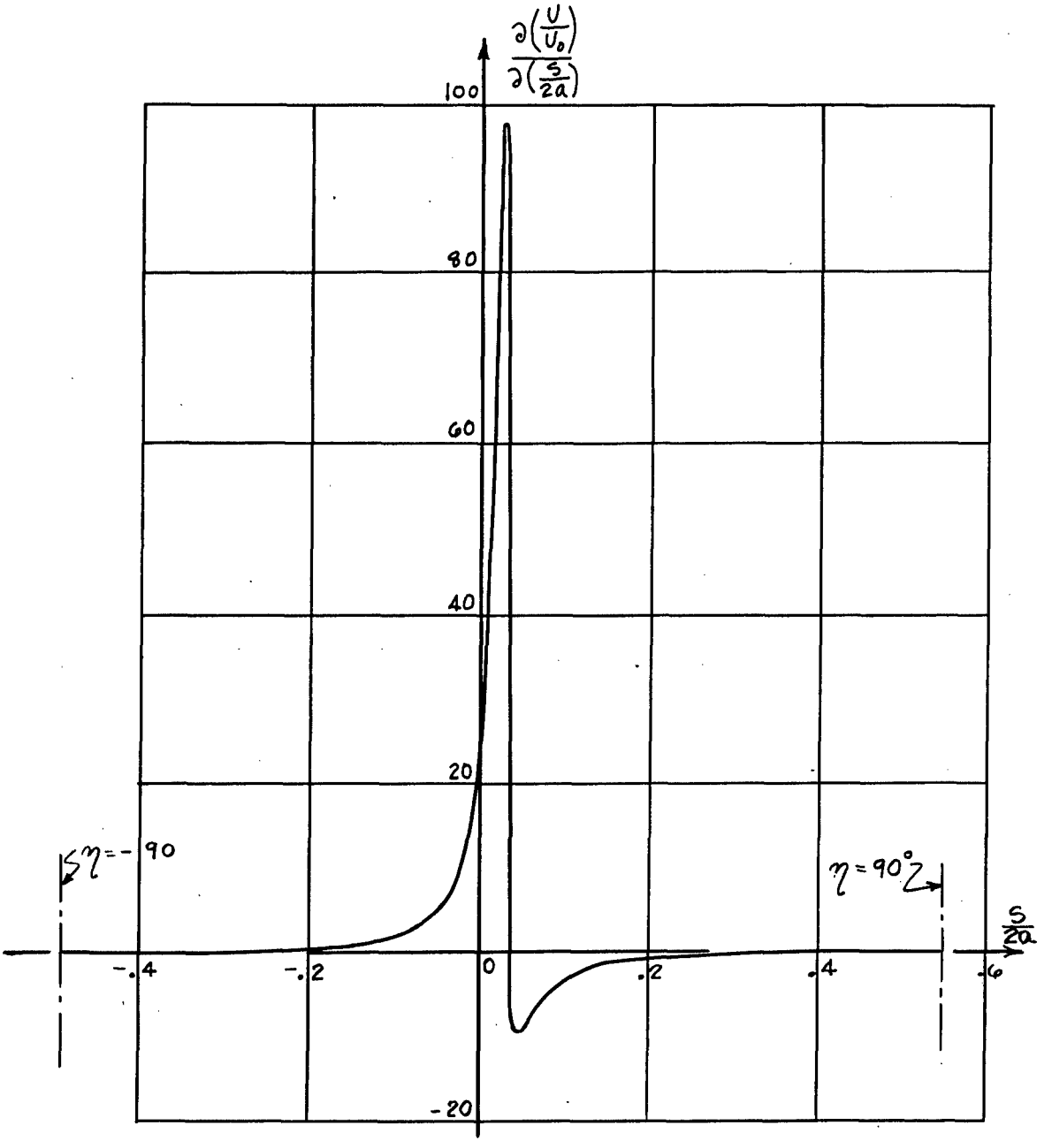

Figure 2.7 Velocity Gradient, $C_L = 2$

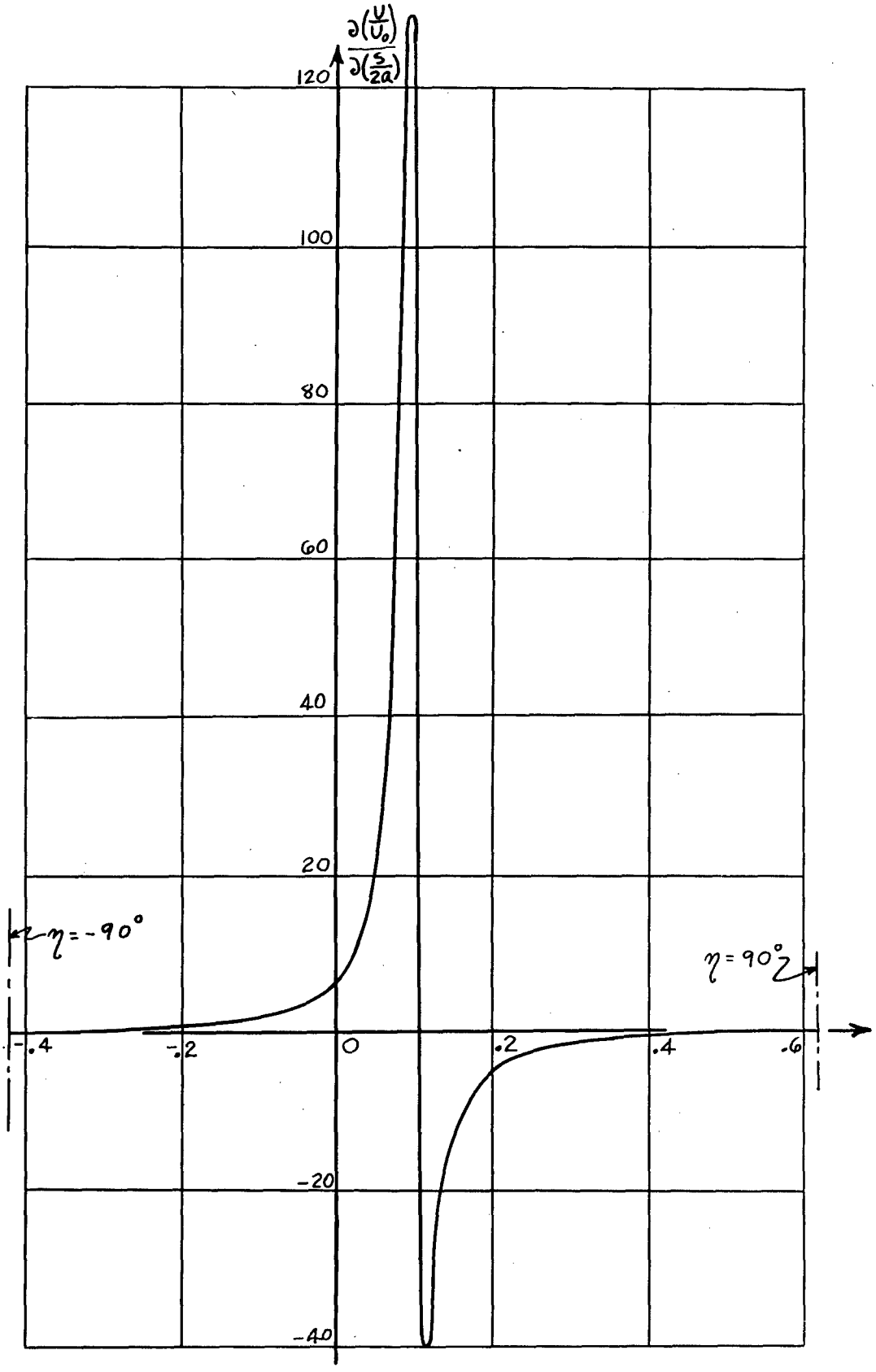

Figure 2.8 Velocity Gradient, $C_L = 4$

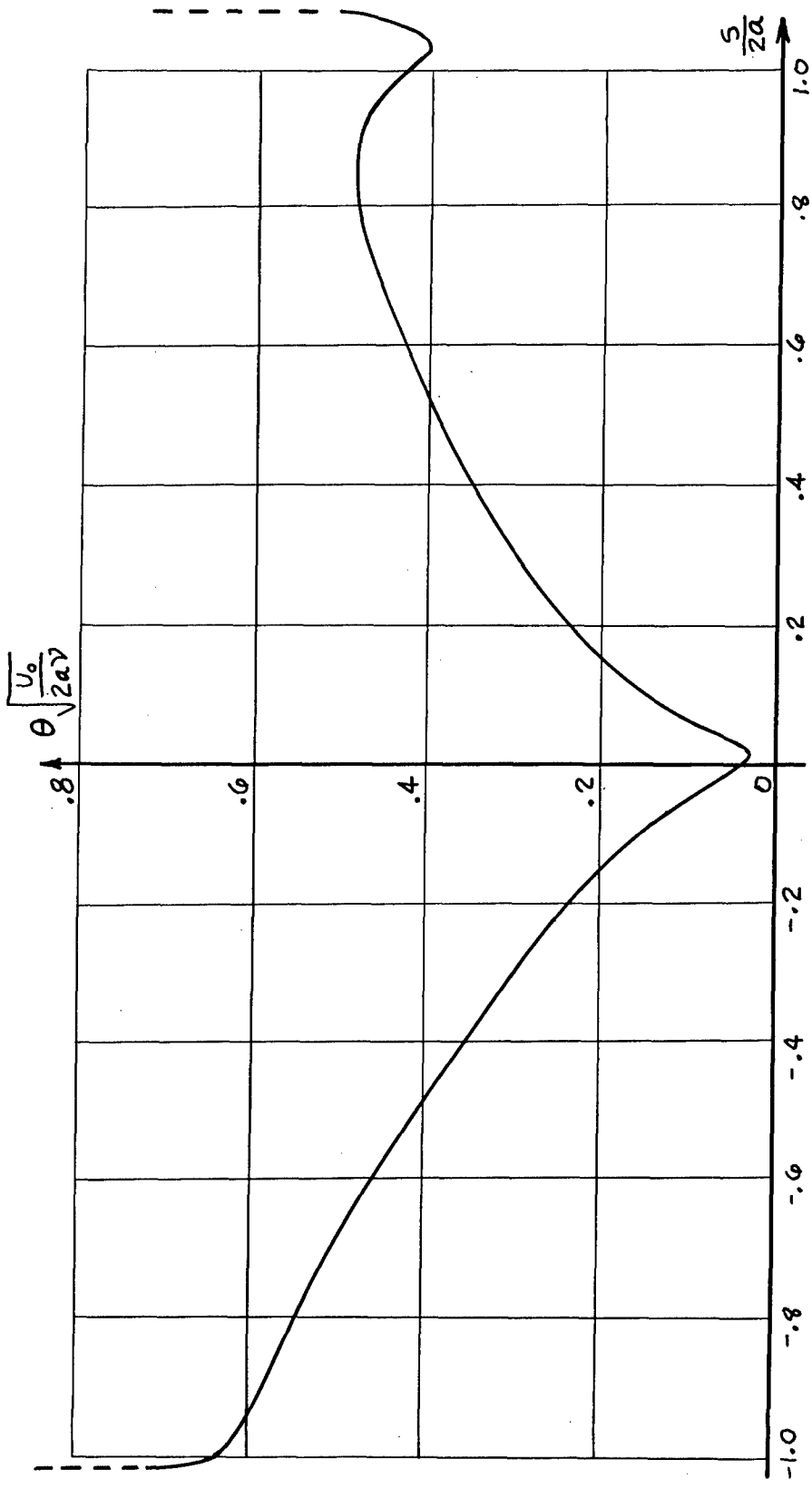

Figure 3.1 Momentum Thickness, $C_L = 1$

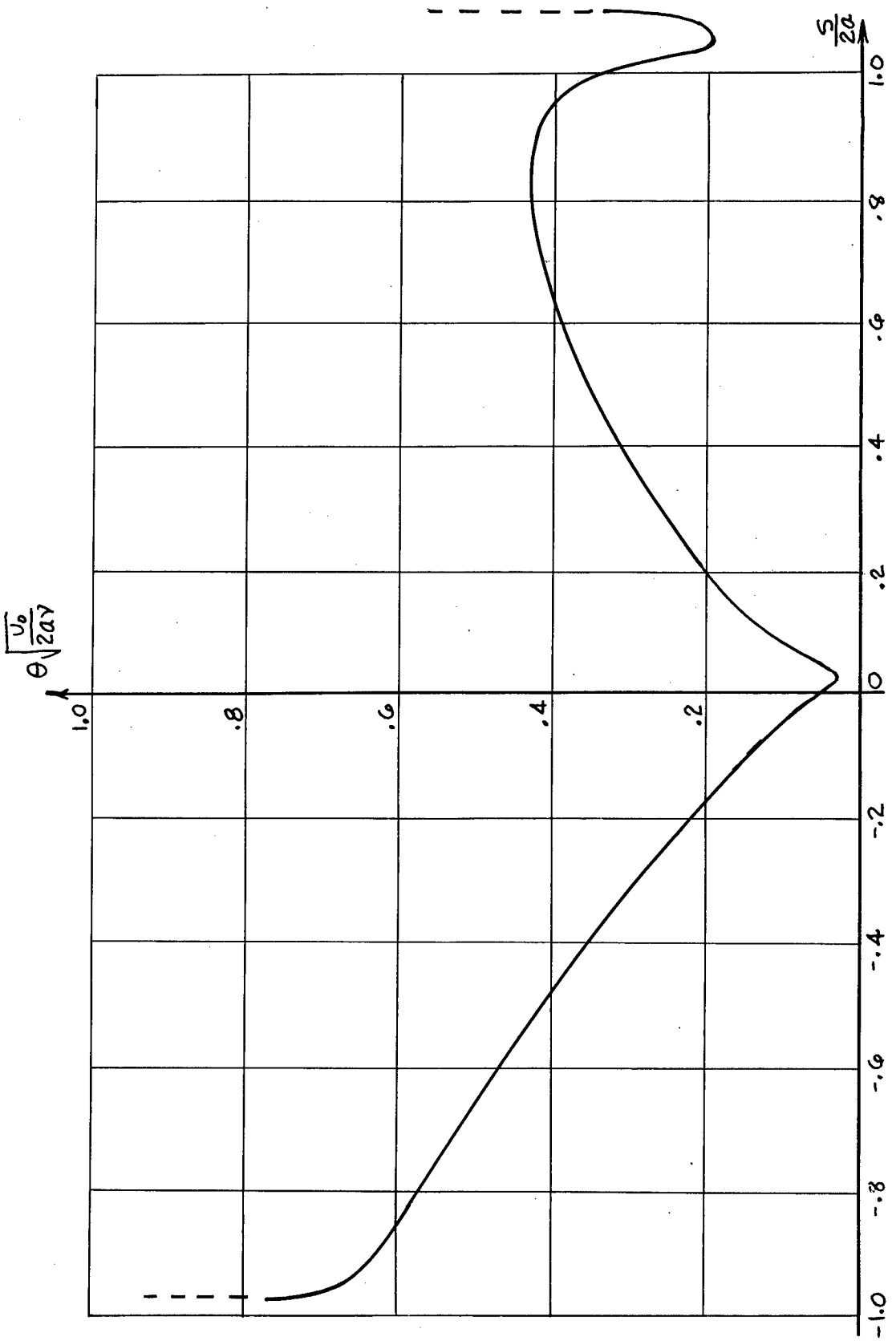

Figure 3.2 Momentum Thickness, $C_L = 2$

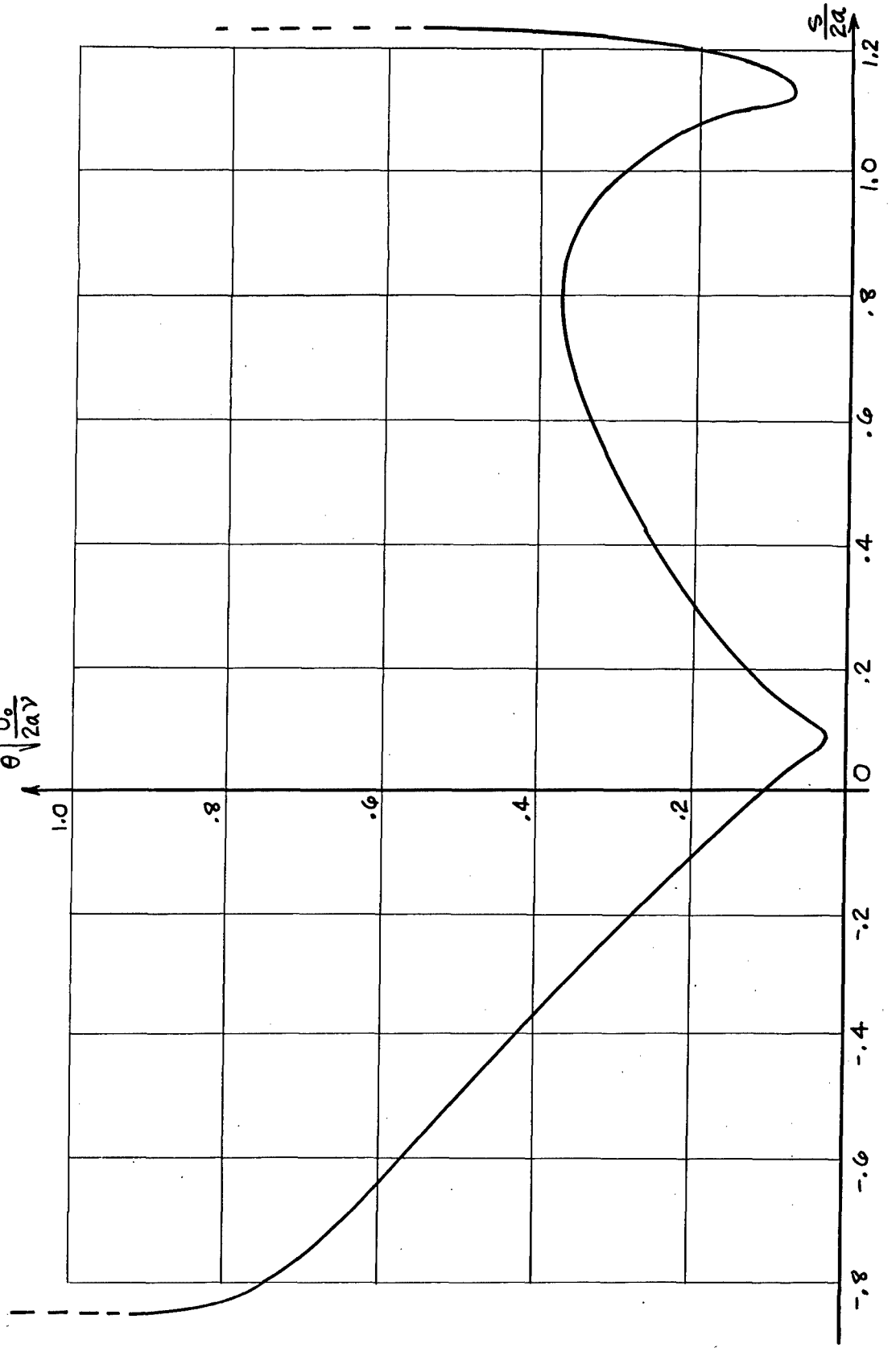

Figure 3.3 Momentum Thickness, $C_L = 4$

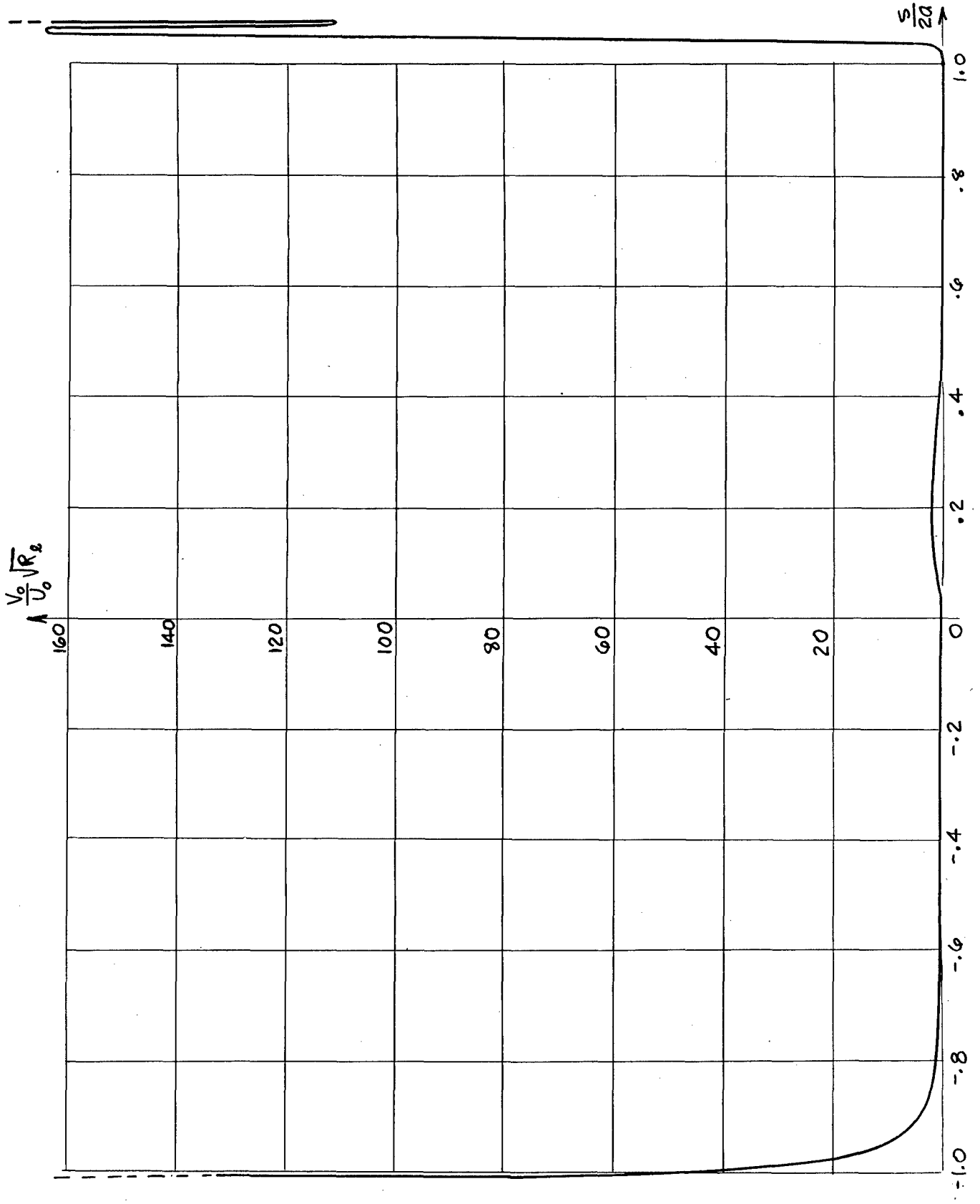

Figure 3.4 Suction Velocity, $C_L = 1$

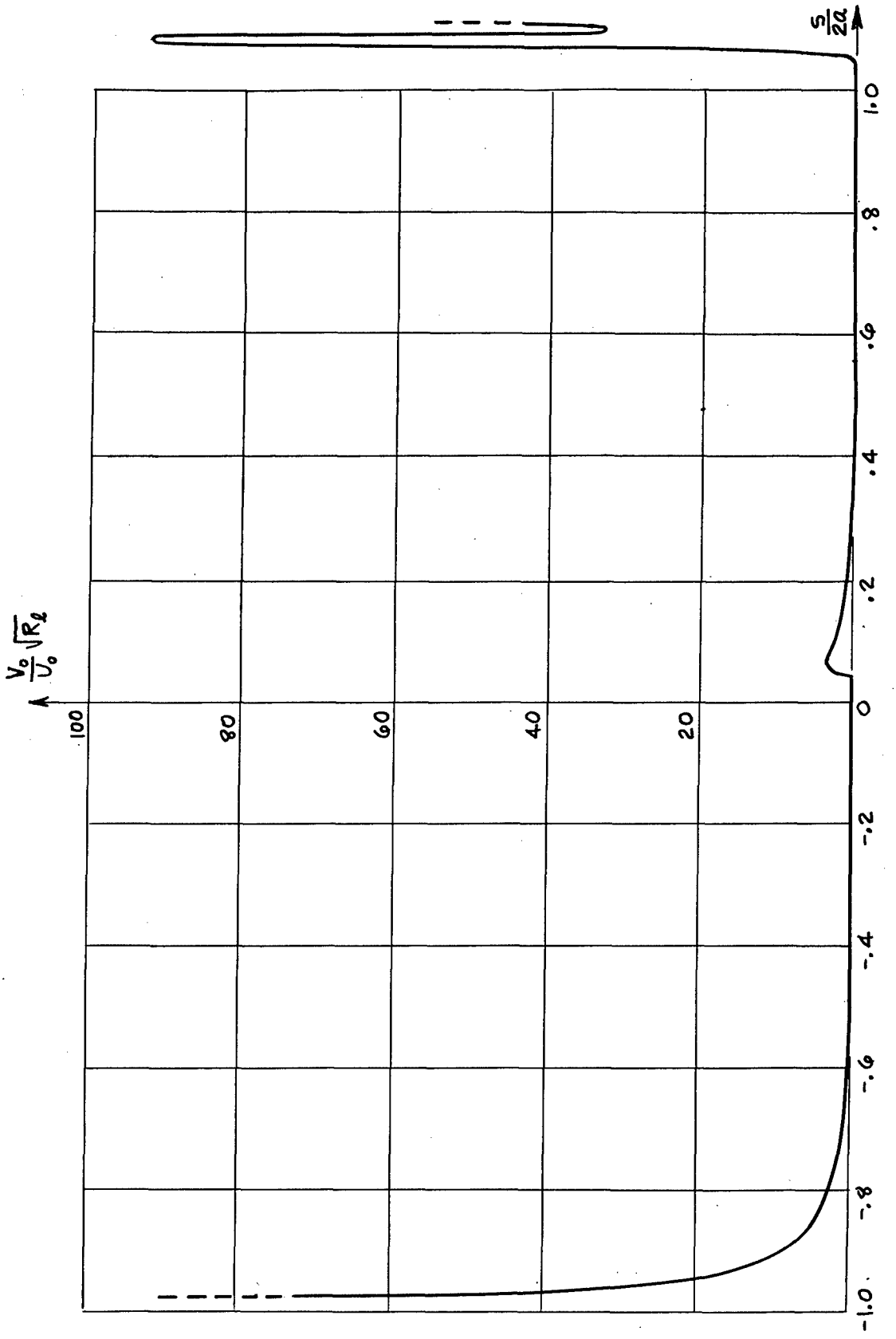

Figure 3.5 Suction Velocity, $C_L = 2$

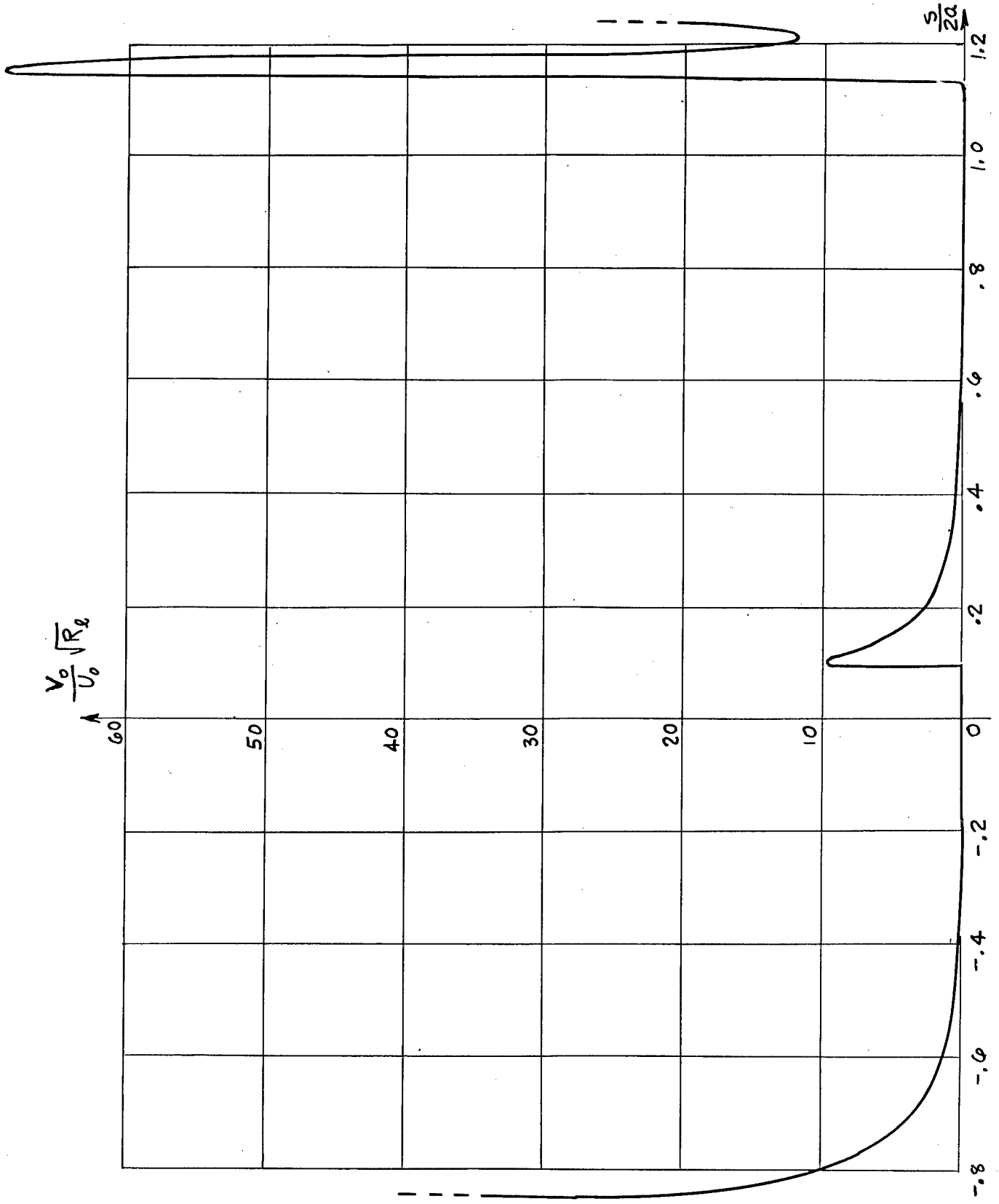

Figure 3.6 Suction Velocity, $C_L = 4$

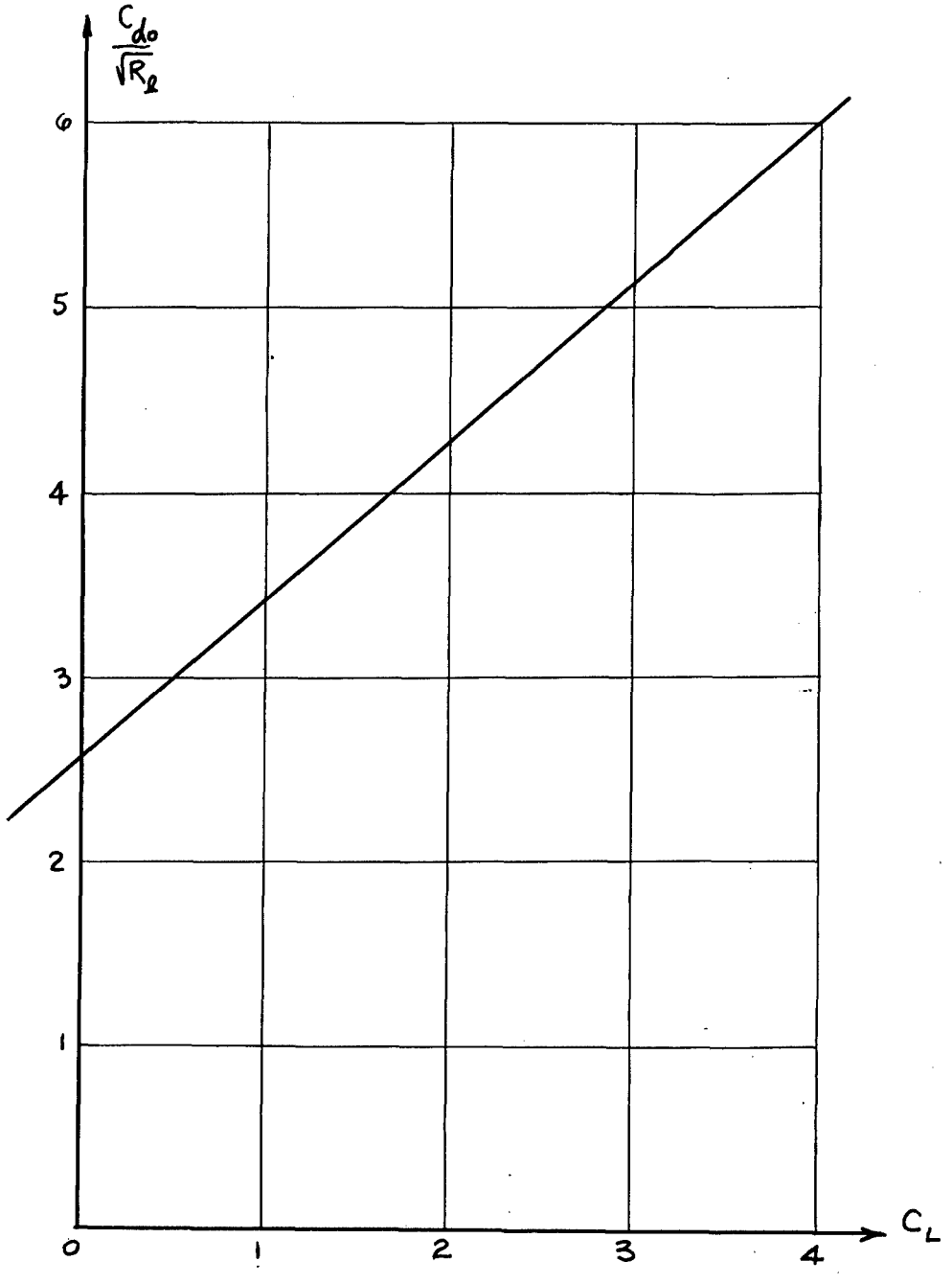

Figure 4.1 Profile Drag Coefficient versus Lift Coefficient

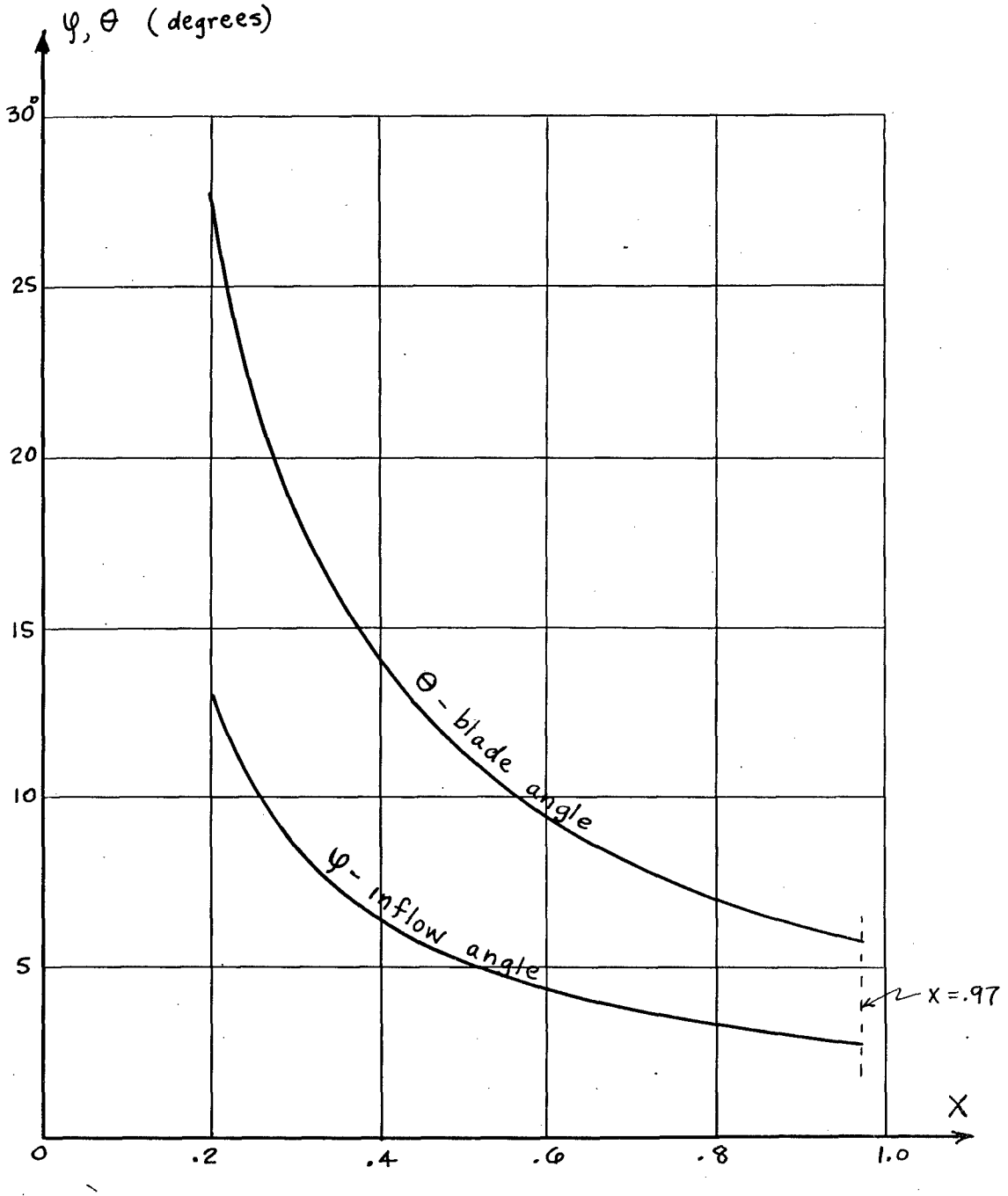

Figure 5.1 Spanwise Variation of Blade Angle and Inflow Angle for Piasecki Rotor

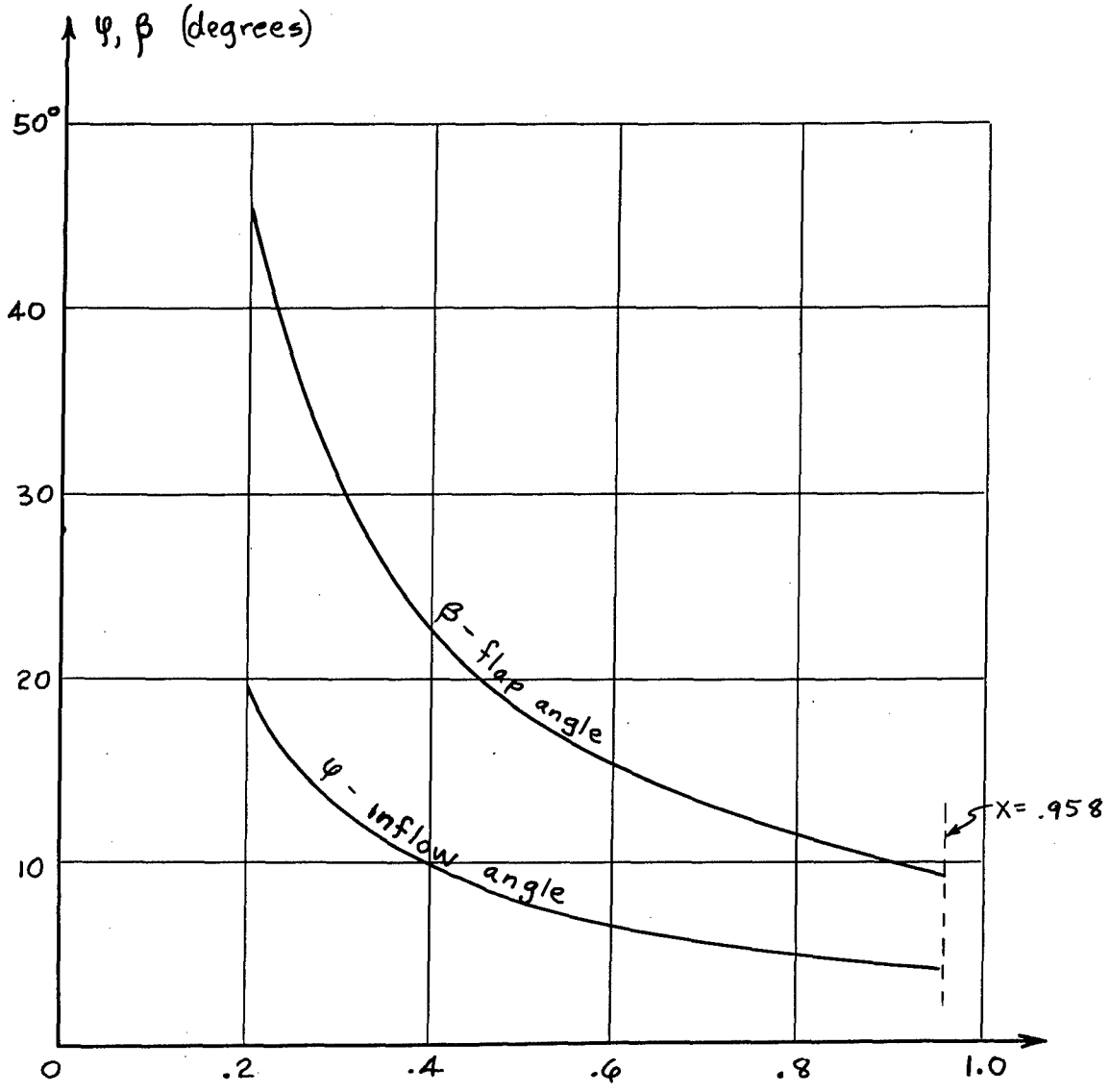

Figure 5.2 Spanwise Variation of Flap Angle and Inflow Angle for Karman-Yuan Rotor

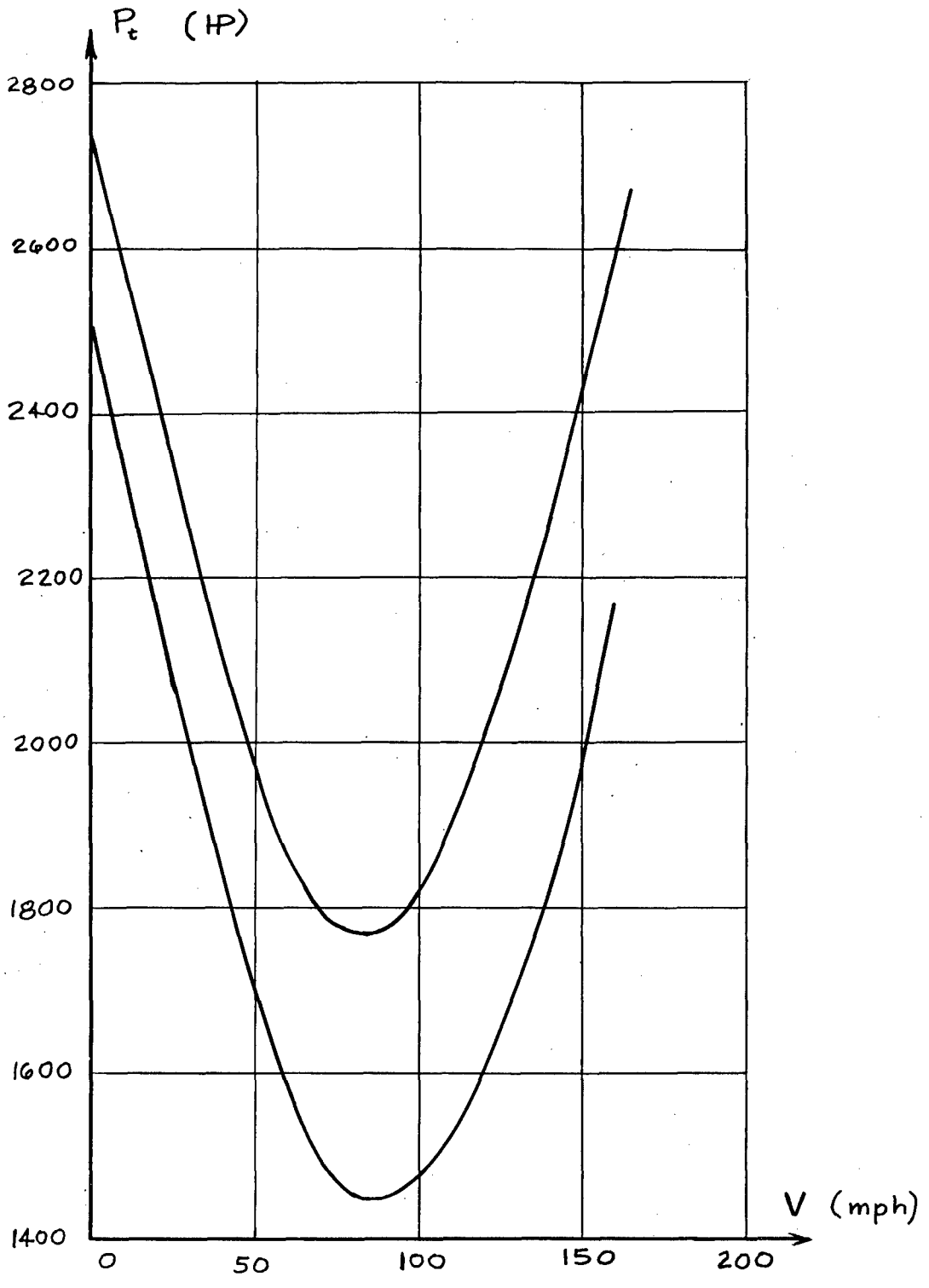

Figure 6.1 Power versus Speed

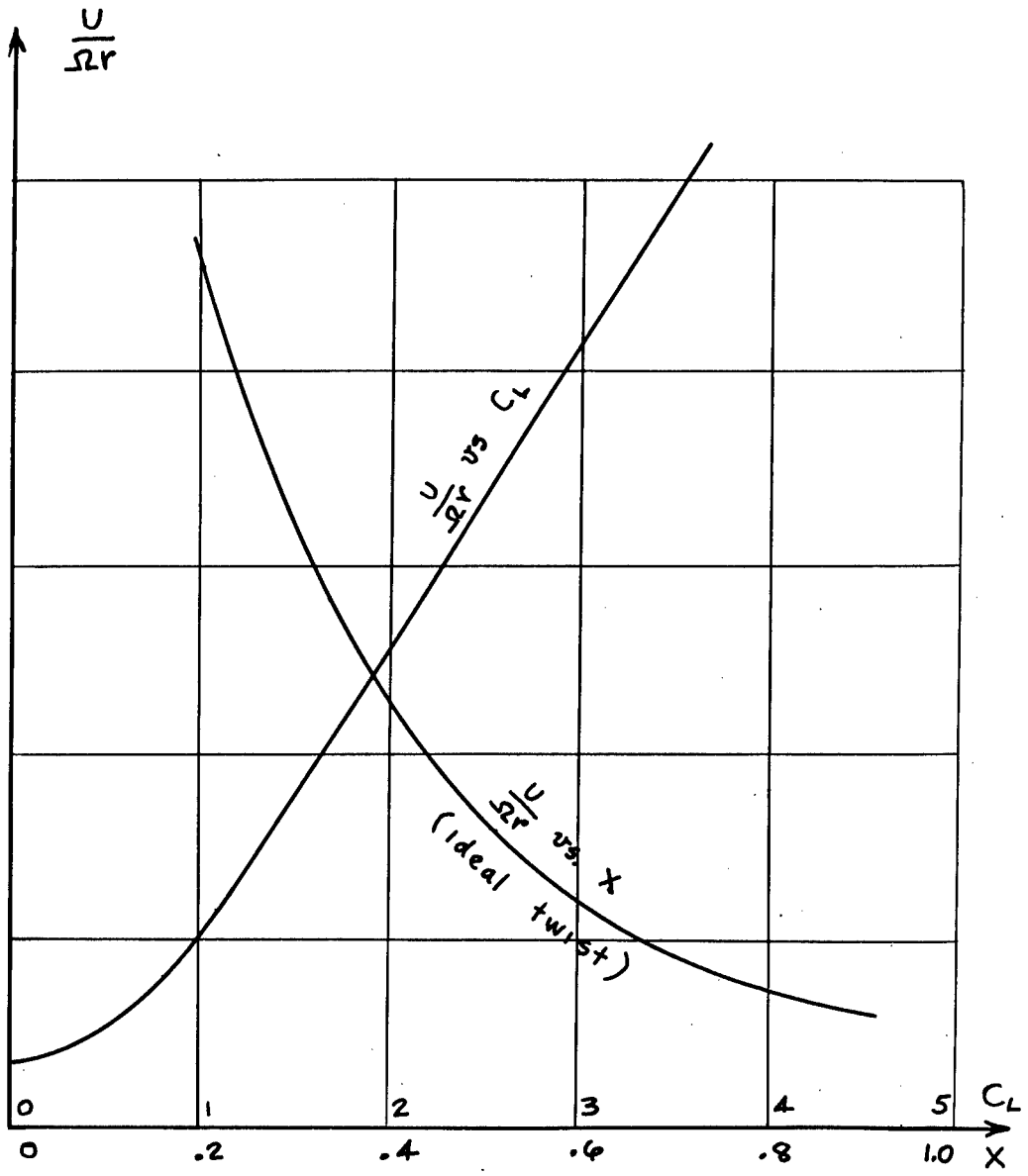

Figure 7.1 $U/\Omega r$ versus x and C_L